論文 / 著書情報
Article / Book Information

題目(和文)	
Title(English)	Cell Penetration and Cell-Selective Drug Delivery Using α-Helix Peptides Conjugated with Gold Nanospheres
著者(和文)	ParkHyejin
Author(English)	Hyejin Park
出典(和文)	学位:博士(工学), 学位授与機関:東京工業大学, 報告番号:甲第9483号, 授与年月日:2014年3月26日, 学位の種別:課程博士, 審査員:三原　久和,中村　聡,和地　正明,小畠　英理,蒲池　利章
Citation(English)	Degree:Doctor (Engineering), Conferring organization: Tokyo Institute of Technology, Report number:甲第9483号, Conferred date:2014/3/26, Degree Type:Course doctor, Examiner:,,,,
学位種別(和文)	博士論文
Type(English)	Doctoral Thesis

Cell Penetration and Cell-Selective Drug Delivery Using α-Helix Peptides Conjugated with Gold Nanospheres

Hyejin Park

Department of Bioengineering

Graduate School of Bioscience and Biotechnology

Tokyo Institute of Technology

Contents

Abbreviations

5-(and-6)-carboxytetramethylrhodamine (TAMRA)

cell counting kit 8 (CCK-8)

cell penetrating (CP) activity

cell penetrating peptide (CPP)

cell penetration (CP) assay

donor bovine serum (DBS)

doxorubicin (DOX)

dulbecco's modified eagle medium (DMEM)

electrospray ionization mass spectrometry (ESI-MS)

fetal bovine serum (FBS)

9-fluorenylmethyloxycarbonyl (Fmoc)

10 nm GNSs (GNS10)

16 nm GNSs (GNS16)

25 nm GNSs (GNS25)

41 nm GNSs (GNS41)

gold nanosphere (GNS)

human immunodeficiency virus transactivating regulatory protein (HIV TAT)

matrix-assisted laser desorption ionization time-of-flight mass spectrometry (MALDI TOF-MS)

N-hydroxybenzotriazole (HOBt)

N-methylpyrrolidone (NMP)

N,N-diisopropylethylamine (DIEA)

nuclear localization signal (NLS)

O-Benzotriazole-N,N,N',N'-tetramethyl-uronium-hexafluorophosphate (HBTU)

penicillin-streptomycin (PS)

peptide-conjugated GNS (P-GNS)

peptide-conjugated 41 nm GNS (P-GNS41)

peptide and doxorubicin conjugated GNS (P-DOX-GNS)

peptide and DOX-PEG conjugated 25 nm GNS (P-DOX-PEG-GNS25)

peptide and PEG conjugated 25 nm GNS (P-PEG-GNS25)

pH-sensitive doxorubicin conjugated PEG (DOX-PEG)

piperidine (PPD)

protein transduction domains (PTD)

quantum dot (QD)

transmission electron microscopy (TEM)

trifluoroacetic acid (TFA)

Chapter 1.

Introduction

1-1 Intracellular drug delivery

Much attention has recently been given to the development of intracellular drug delivery systems, which hold promising applications for human disease care [1]. However, payload across the plasma membrane is still challenging. Eukaryotic cells are coated with a plasma membrane, which selectively penetrates ions and organic molecules through ion channels and transporters and restricts such molecular transfer from outside environment. This membrane is an obstacle to the transfer of drugs or gene medicines to the inside of cells.

To overcome this barrier, carrier-based intracellular delivery has been investigated using viral vectors [2], such as the retrovirus, lentivirus, herpes simplex virus and adenovirus, and non-viral vectors [3], such as liposome, cationic polymers and cell penetrating peptides (CPPs) [4-7]. The viral vectors and non-viral vectors have the advantages and disadvantages. The viral vectors can expect high delivery efficiency. However, viral vectors show the high toxicity and affect to immune system. On the other hands, delivery efficiency of non-viral vectors is less than viral vectors. However, they have low toxicity and immunogenicity.

These vectors deliver the cargo into cells like direct penetration or endocytosis mediated entry [8-12]. Direction penetration is an energy-independent cellular process, which is occurred translocation across the cell membrane by interaction with phospholipid bilayer. Endocytosis is an energy-dependent process and they were principally categorized in three types by mechanism, clathrin-mediated endocytosis, caveolae mediated endocytosis, and macropinocytosis (Figure 1-1). Clathrin mediated endocytosis is a major mechanism for the internalization of membrane receptors into cells. A specific molecule is bound with receptor or ion-channel on the plasma membrane. After binding, cytosolic

protein clathrin forms a vesicle by coating on the inner surface of the cell membrane and internalized. Caveolae mediated endocytosis is one of the clathrin independent endocytosis. The cholesterol, sphingolipid-rich plasma membrane invagination of a diameter of 50–80 nm was involved for the internalization, of which caveolin-1 is the main protein component required. Macropinocytosis is non-specific endocytosis of solute macromolecules and forms a vesicle: macropinosome. After internalizing, the vesicle is thought to eventually fuse with lysosomes or recycle its content to the surface. The problem, however, is that every molecule/particle entering in cell via the endocytic pathway becomes entrapped into endosome and eventually ends in lysosome, and only a small fraction of unaffected substance appears in the cell cytoplasm. As a result, many compounds showing a promising potential in vitro, cannot be applied in vivo owing to bioavailability problems. Several factors are required for the successful application of these systems: 1) high internalization efficiency, 2) a high payload of drugs, 3) non-degradation of the drugs in extra- and intra-cellular space, and 4) low toxicity and immunogenicity. The construction of effective intracellular drug delivery system would be a great element for disease cure, especially cancer therapy improving chemotherapy efficacy and reducing side effects of drugs.

In this study, peptides of Mihara group and gold nanoparticles were used for construction of a cell selective drug delivery system.

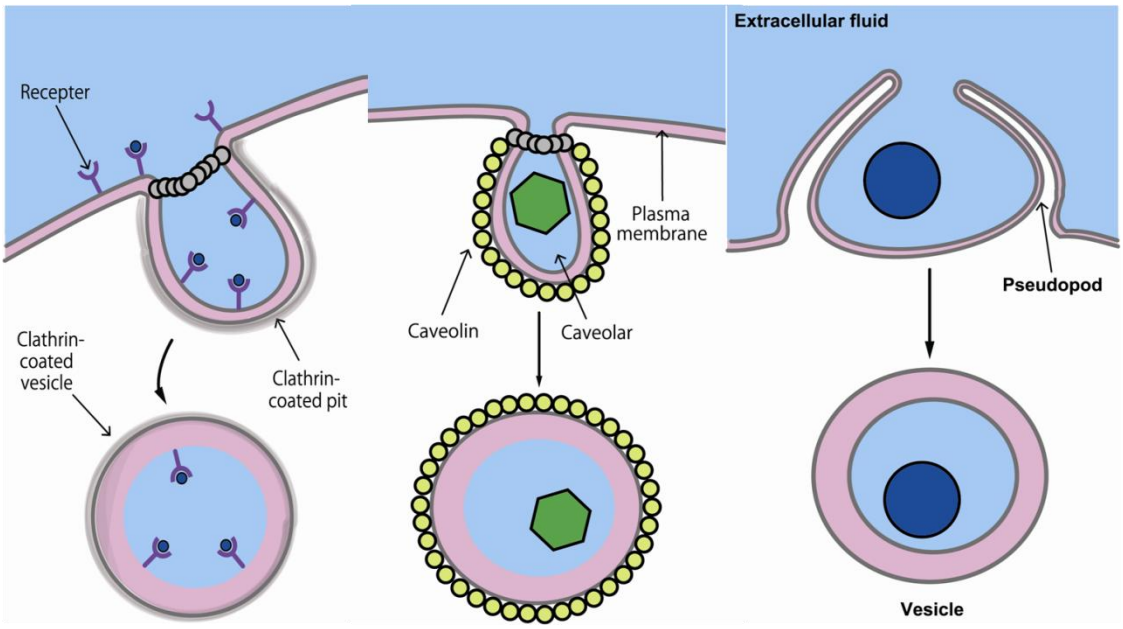

Figure 1-1. Illustration of endocytosis: clathrin-mediated endocytosis (left), caveolae mediated endocytosis (middle), and macropinocytosis (right) [11,12].

1-2 Cell penetrating peptides (CPPs)

Figure 1-2 shows typical CPPs. Typical CPPs that have been functionally studied include the human immunodeficiency virus transactivating regulatory protein (HIV TAT), the 16-amino acid peptide penetratin and transportan derived from protein transduction domains (PTD), MPG, MAP and KALA of amphiphilic peptides and polyarginine peptides [4-6]. These peptides are positively charged by rich in lysine or arginine residues or have amphiphilic properties. It has been proposed that CPPs are penetrated inside cell by endocytosis or endocytosis-independent direct penetration through the plasma membrane [8-12], although the detailed mechanisms of the internalization of CPPs are not well understood. Moreover, because CPPs are capable of transporting attached macromolecules from the extracellular space through the cell membrane into the cytoplasm, they have been developed as vectors for molecular delivery into various cells.

CPPs were delivered inside cells conjugated with genes, proteins [13-15] and drugs such as anti-cancer drugs and protein drugs [15-18], and they have been used for gene, protein therapy, drug delivery, and cancer treatment by releasing them in cytoplasm or nucleus. The imaging agents such as quantum dots (QDs) and dendrimeric nanoparticles conjugated CPPs [19,20] have also been researched for molecular imaging, targeted therapy and in vivo study. These peptides showed the high cell penetrating (CP) activity; however, they have low cell selectivity. Thus, CPPs with high internalization, cell specificity, and low cytotoxicity have been considered to increase the applicability as biomaterials for medical application.

Mihara group constructed an α-helix peptide library (Figure 1-3) [21-24] and systematically assayed the cell uptake of synthetic α-helical peptides by conjugating the fluorescent dye at N-terminus in four cell lines. They showed the characteristic and

different CP activity against four cell lines, HeLa, A549, 3T3-L1, and PC12 (Figure 1-4) [24]. In this study, four peptides (RF, RA, EF, and EA), which are different one or two amino acids among 16 amino acids sequence and showed the different CP activity, were selected from the α-helix peptide library [21-24].

Name	Sequences
Cationic	
Tat (48-60)	GRKKRRQRRRPQ
Penetratin	RQIKIWFQNRRMKWKK
Polyarginines	R_n
Amphipathic	
KALA	WEAKLAKALAKALAKHLAKALAKALKALKACEA
MPG	GALFLGFLGAAGSTMGAWSQPKKKRKV
Transportan	GWTLNSAGYLLGKINLKALAALAKKIL
MAP	KLALKLALKAALKLA

Figure 1-2. Typical CPPs

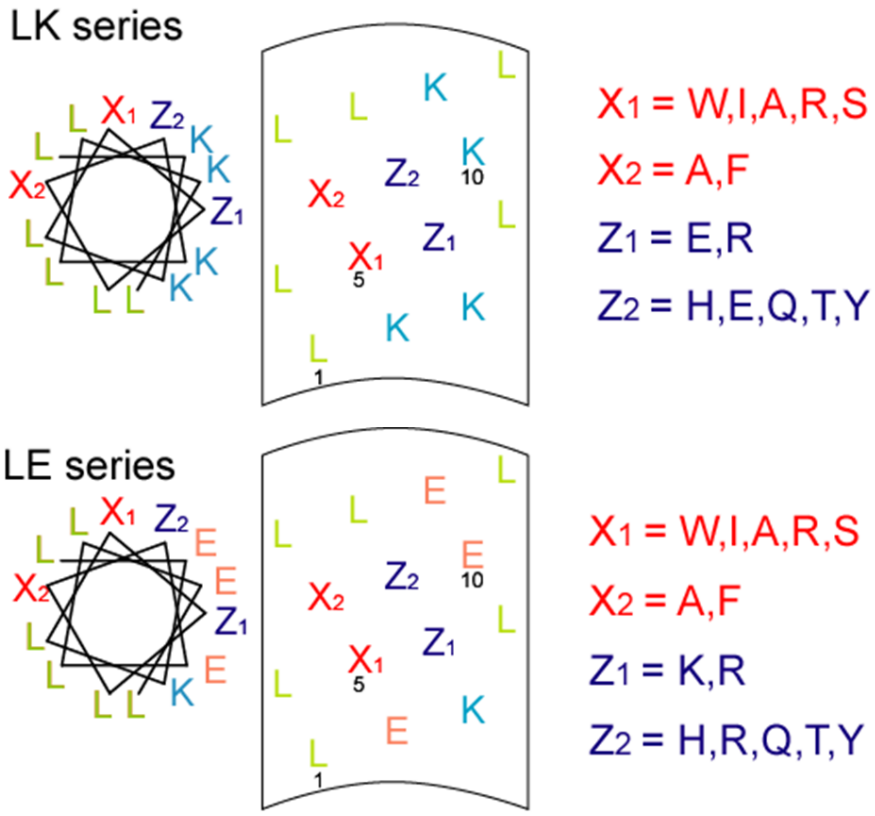

Figure 1-3. Construction of the peptide library consisting of 202 α-helical peptides. Designed peptides in which four residues (X1, Z1, X2, and Z2) in the central region of LKKLLKLLKKLLKL (L8K6; No.000) and LEKLLELLKELLEL (No. 201 L8K2E4) were replaced with other amino acids to give 101 LK peptides and 101 LE peptides [21-24].

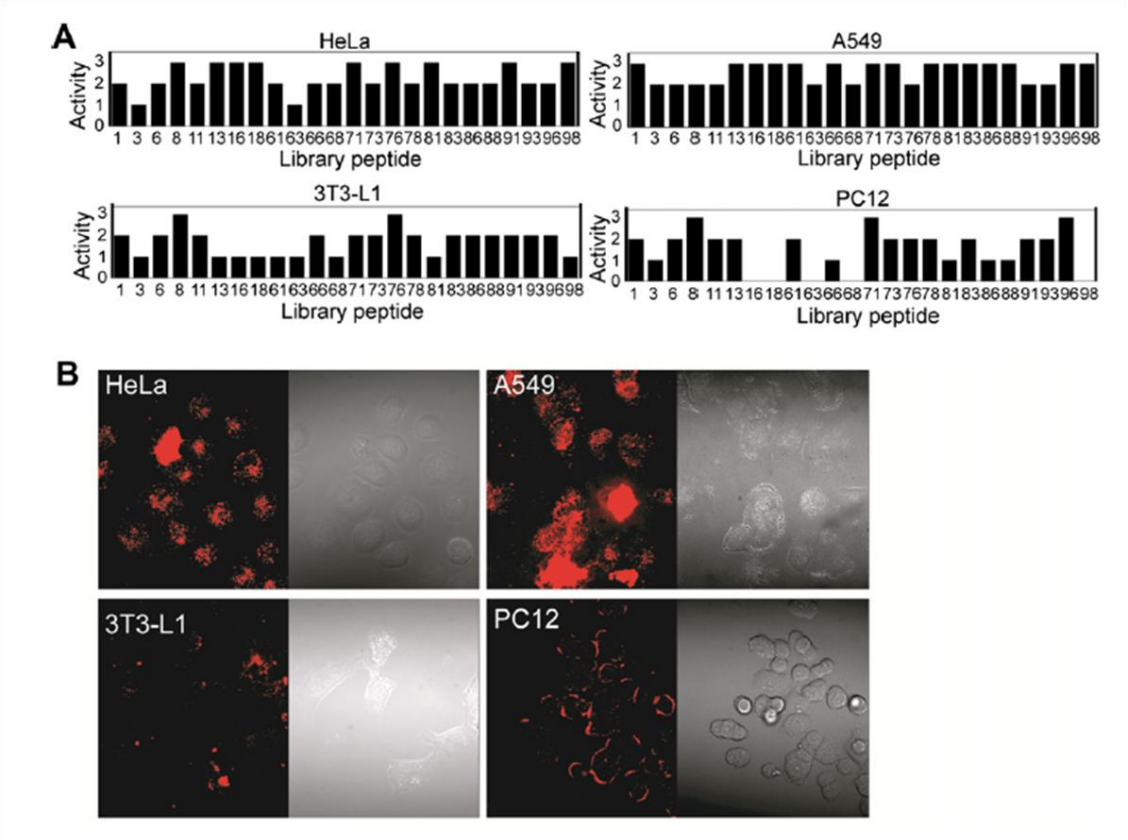

Figure 1-4. Cell penetration (CP) assay in multiple cell types. (a) CP activities of the 24 library peptides to HeLa, A549, 3T3-L1 and PC12 cells (cells incubated for 1 h with peptides at a final concentration of 2 μM at 37 ℃). (b) Confocal micrographs of four cells with 2 μM No. 018 peptide; rank 3 for HeLa, rank 3 for A549, rank 1 for 3T3-L1, rank 0 for PC12 [24].

1-3 Nanoparticles

Molecular imaging is a promising technique evaluating of molecular changes, gene expression and biochemical changes in cells. Using this technique, medical applications such as early detection and treatment of diseases would be possible owing to occurring biochemical or molecular genetics changes with disease. In addition, molecular imaging is not only a non-invasive method but also allows quantitative tests. It would be a good tool in field of the diagnosis of diseases such as cancer, neurological and cardiovascular diseases.

Organic fluorescent dyes have been widely used for molecular imaging in chemical and cellular biology. However, due to intrinsic limitations, such as insolubility and photobleaching [25-27], they are not useful for long-term imaging studies. Because of these problems, much attention has been focused on nanometer sized particles, such as gold and silver nanoparticles, QDs, and magnetic particles. These particles show good physicochemical properties according to their sizes and shapes and have potentials in the fields of biosensing [28], bioimaging [29-32], and drug delivery [33]. Although QDs are limited by cytotoxicity against biosamples [34], they have been used for in vivo applications by reducing the cytotoxicity using coating materials like PEG [29,35].

Among nanoparticles, gold nanospheres (GNSs) are the most studied nanomaterials, because they have advantages such as biocompatibility, high solubility, easiness of synthesis and bioconjugation, and physical properties such as strong absorption and scattering. Figure 1-5 shows the typical study fields using GNSs: biosensing [36-38], molecular imaging [30,31], in vivo study [39-41] and drug delivery [42,43]. GNSs were used for DNA or protein sensing study to improve sensitivity. For examples, colorimetric detection is a rapid and convenient method of a homogeneous assay format using strong

surface plasmon absorption of GNS [37]. In addition, SPR biosensors utilized with GNS immobilized on the substrate or on the target and receptor molecules for the amplification of mass [36,38]. GNSs in biosensor have applicability for high throughput or multiplex detection of biomarkers. GNSs were also used as cellular imaging agents and carrier for drug delivery inside cells [33,42]. Functionalized GNS showed the applicability for cancer diagnosis and therapy detecting the target molecules such as cancer markers [30,31]. A GNS based system was already successful in tumor detection in vivo using near-infrared optical imaging [40-42] and surface enhanced raman scattering technique [39] in tumor bearing mouse. It is thought that GNSs are suitable for bioapplication from these studies. In this study, four sizes of GNSs were synthesized and examined for cellular imaging and drug delivery application.

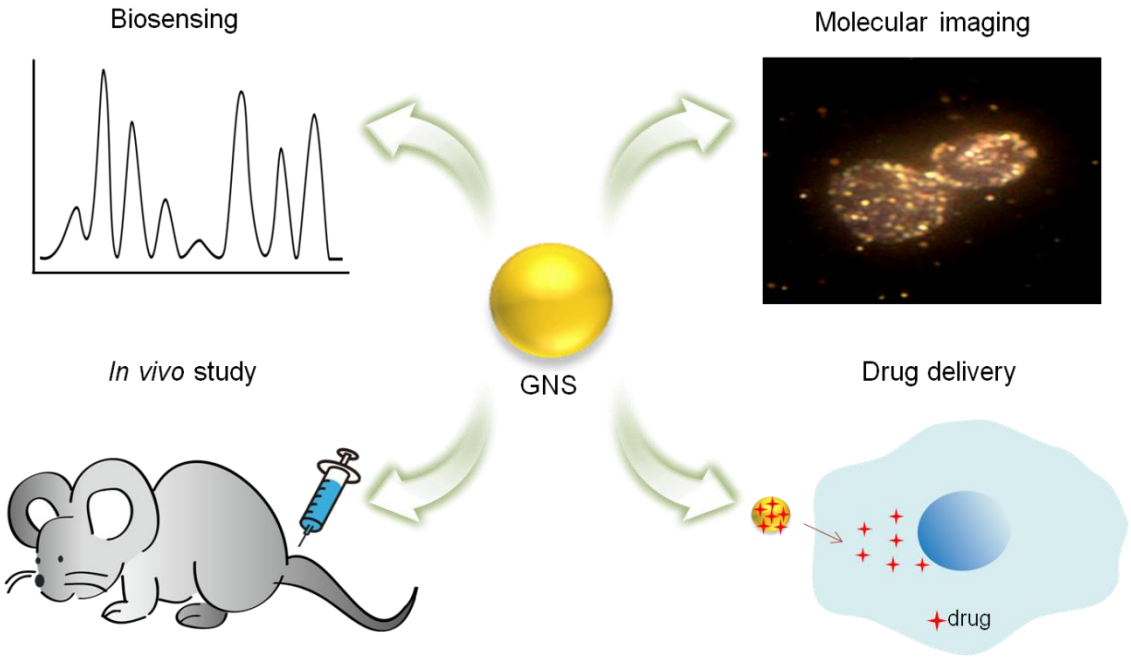

Figure 1-5. Application fields using GNS: biosensing, molecular imaging, in vivo study and drug delivery.

1-4 The purpose of this thesis

Cell selective drug delivery system is essential for the development of cancer therapy technologies. A CPPs based delivery system, which can enter inside cell through the cell membrane, have been focused and could be useful in the research fields of drug delivery, gene therapy, and cancer therapy. They have, however, the problems such as low cell selectivity, low CP activity, and cell toxicity. In this study, to solve the these disadvantages, peptides were selected from a 16-amino acid peptide library developed in Mihara group, which showed different CP activity against four cell lines, although these peptides had only one or two amino acid differences among 16 amino acids. A fluorescent dye conjugated with CPPs in the previous research in Mihara group [24] was changed to GNS for designing the nanoprobes. The GNS would function as an imaging agent with multi-peptide conjugation for cell interactions. The purpose of this thesis is construction and evaluation of a novel drug delivery system using two materials: α-helical CPP and GNS (Figure 1-6).

In chapter 2, α-helix peptides conjugated GNSs (P-GNSs) were constructed for the cell selective drug delivery system by conjugating peptide with four sizes GNSs (10, 16, 25, 41 nm) to compare the peptide conjugation amount against GNSs size. Among them, 41 nm GNSs (GNS41) were conjugated with the largest amount of peptide per particle and showed the low cytotoxicity.

In Chapter 3, applicability of cell selective drug delivery was investigated using P-GNS41. The CP activity in three cell lines and cell death induction by conjugating an anti-cancer drug on the GNS surface were evaluated [43]. Peptides containing Cys at the C- or N- terminus were conjugated with GNS41, and the cell internalization properties of these complexes were examined. P-GNSs41 displayed the characteristic CP activity depending

on the amino acid sequence with enhanced penetrability. Furthermore, the applicability of P-GNSs41 to drug delivery was examined in three cell lines by conjugating doxorubicin (DOX) onto the GNS41 surface (P-DOX-GNS) [44]. DOX is an anti-cancer drug that intercalates with DNA and inhibits macromolecular biosynthesis. The potential of P-GNS41 for the cell-selective drug delivery and the use of P-DOX-GNS41 in selective induction of cell death were examined.

In chapter 4, the feasibility of using 25 nm GNS instead of 41 nm GNS was examined for nuclear targeting to get the higher cell death induction than P-GNS41. Five nanoprobes conjugated to either the TAT peptide or one of four peptides from the 16-amino acid peptide library (P-GNS25). These five nanoprobes were coated with PEG (P-PEG-GNS25) to maintain the high stability during long incubations for nuclear targeting. P-PEG-GNSs are expected to be taken up by the cell via endocytosis, and the P-PEG-GNSs in endosomes or lysosomes may then migrate to the nucleus. Therefore, a pH-sensitive DOX-PEG is synthesized using a hydrazone linkage and conjugated to a 25 nm GNS (P-DOX-PEG-GNS25) to allow the controlled release of DOX from the vesicles under pH 5 [45-47]. A more efficient cell-selective drug delivery system than that of P-GNS41 was demonstrated by examining the CP activities of five constructed P-PEG-GNS25 nanoprobes and the cell death activities of P-DOX-PEG-GNS25 and then comparing the results with the activities of the TAT peptide.

In chapter 5, conclusions and future prospects of this thesis were described.

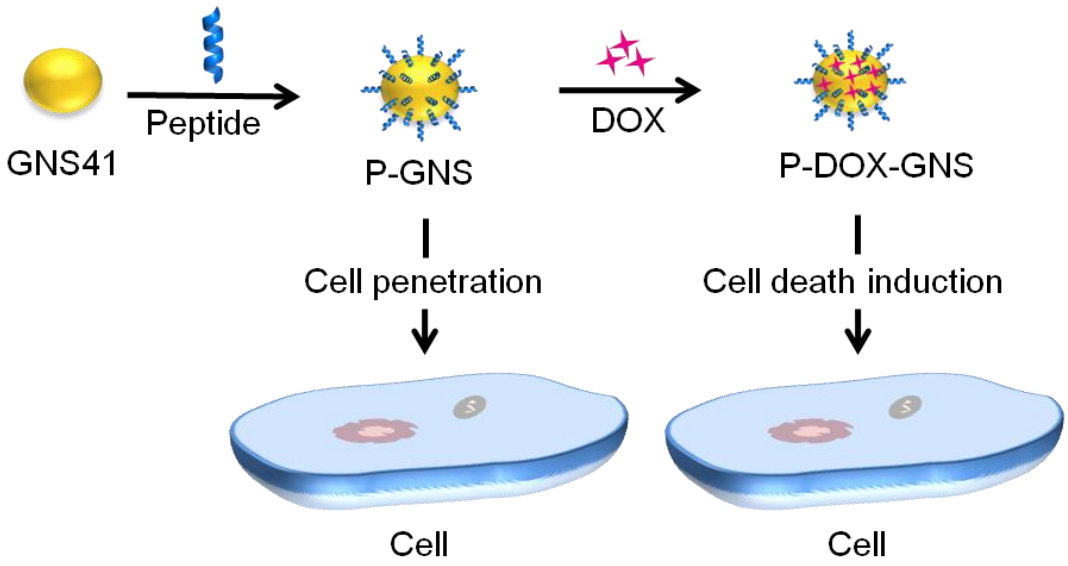

Figure 1-6. Illustration of thesis purpose. P-GNS and P-DOX-GNS were constructed and evaluated in applicability by examining the CP activities and cell death induction with DOX.

Reference

[1] Torchilin V. Intracellular delivery of protein and peptide therapeutics. Drug discovery today 2008; 5: e95-103.

[2] Thomas C.E., Ehrhardt A., Kay M.A. Progress and problems with the use of viral vectors for gene therapy. Nat rev Genet 2003; 4: 346-58.

[3] Niidome T, Huang L. Gene therapy progress and prospects: Nonviral vectors. Gene Ther 2002; 9: 1647-52.

[4] Lindgren M, Hällbrink M, Prochiantz A, Langel Ü. Cell-penetrating peptides. Trends Pharmacol Sci 2000; 21: 99-103.

[5] Hansen M, Kilk K, Langel Ü. Predicting cell-penetrating peptides. Adv Drug Deliver Rev 2008; 60: 572-9.

[6] Futaki S. Membrane-permeable arginine-rich peptides and the translocation mechanism. Adv Drug Deliver Rev 2005; 57: 547-58.

[7] Jiang T, Zhang Z, Zhang Y, Lv H, Zhou J, Li C, et al. Dual-functional liposomes based on pH-responsive cell-penetrating peptide and hyaluronic acid for tumor-targeted anticancer drug delivery. Biomaterials 2012; 33: 9246–58.

[8] Fischer PM. Cellular uptake mechanisms and potential therapeutic utility of peptidic cell delivery vectors: Progress 2001-2006. Med Res Rev 2007; 27: 755–95.

[9] Herce H.D., Garcia A.E. Cell penetrating peptides: How do they do it?. J Biol Phys 2007; 33: 345–56.

[10] Deshayes S, Morris M.C., Divita G, Heitz F. Cell-penetrating peptides: tools for intracellular delivery of therapeutics. Cell Mol Life Sci 2005; 62: 1839-49.

[11] Hillaireau H, Couvreur P. Nanocarriers entry into the cell: relevance to drug delivery. Cell Mol Life Sci 2009; 66: 2873–96

[12] Petros RA, DeSimone JM. Strategies in the design of nanoparticles for therapeutic applications. Nat Rev Drug Discov 2010; 9: 615-27

[13] Eguchi A, Dowdy SF. siRNA delivery using peptide transduction domains. Trends Pharmacol Sci 2009; 30: 341–45.

[14] Xia H, Mao Q, Davidson B.L. The HIV tat protein transduction domain improves the biodistribution of β-glucuronidase expressed from recombinant viral vectors. Nat Biotechnol 2001; 19: 640-4.

[15] Wadia JS, Dowdy SF. Transmembrane delivery of protein and peptide drugs by tat-mediated transduction in the treatment of cancer. Adv Drug Deliver Rev 2005; 57: 579–96.

[16] Pero SC, Shukla GS, Cookson MM, Flemer Jr S, Krag DN. Combination treatment with Grb7 peptide and doxorubicin or trastuzumab (herceptin) results in cooperative cell growth inhibition in breast cancer cells. British Journal of Cancer 2007; 96: 1520-5.

[17] Bolhassani A. Potential efficacy of cell-penetrating peptides for nucleic acid and drug delivery in cancer. Biochimica et Biophysica Acta 2011; 1816: 232-46.

[18] Snyder EL, Dowdy SF. Cell penetrating peptides in drug delivery. Pharm Res-Dordr 2004; 21: 389-93.

[19] Olsona ES, Jianga T, Aguileraa TA, Nguyend QT, Elliese LG, Scadeng M, et al. Activatable cell penetrating peptides linked to nanoparticles as dual probes for in vivo fluorescence and MR imaging of proteases. Proc Natl Acad Sci 2010; 107: 4311–6.

[20] Ruan G, Agrawal A, Marcus AI, Nie S. Imaging and tracking of tat peptide-conjugated quantum dots in living cells: new insights into nanoparticle uptake, intracellular transport, and vesicle shedding J Am Chem Soc 2007; 129: 14759-66.

[21] Usui K, Tomozaki K, Mihara H. Protein-fingerprint data mining of a designed α-helical peptide array. Mol BioSyst 2006; 2: 417-20.

[22] Usui K, Tomozaki K, Mihara H. Screening of a-helical peptide ligands controlling a calcineurin-phosphatase activity. Bioorg Med Chem Lett 2007; 17: 167-71.

[23] Usui K, Kakiyama T, Tomozaki K, Mie M, Kobatake E, Mihara H. Cell fingerprint patterns using designed a-helical peptides to screen for cell-specific toxicity. Bioorg Med Chem Lett 2011; 21: 6281-4.

[24] Usui K, Kikuchi T, Mie M, Kobatake E, Mihara H. Systematic screening of the cellular penetration of designed alpha-helix peptides. Bioorg Med Chem 2013; 21: 2560-67.

[25] Song L, Varma CA, Verhoeven JW, Tanke HJ. Influence of the triplet excited state on the photobleaching kinetics of fluorescein in microscopy. Biophys J 1996; 70: 2959–68.

[26] Song L, Van Gijlswijk RP, Young IT, Tanke HJ. Influence of fluorochrome labeling density on the photobleaching kinetics of fluorescein in microscopy. Cytom Part A 1997; 27: 213–23.

[27] Bernas T, Zarebski M, Cook RR, Dobrucki JW, Cook PR. Minimizing photobleaching during confocal microscopy of fluorescent probes bound to chromatin: role of anoxia and photon flux. J Microsc-Oxford 2004; 215: 281–96.

[28] Song S, Qin Y, He Y, Huang Q, Fan C, Chen HY. Functional nanoprobes for ultrasensitive detection of biomolecules. Chem Soc Rev 2004; 39: 4234–43.

[29] Gao X, Cui Y. Levenson RM, Chung LWK, Nie S. In vivo cancer targeting and imaging with semiconductor quantum dots. Nat Biotechnol 2010; 22: 969–76.

[30] El-Sayed IH, Huag X., El-Sayed MA. Surface plasmon resonance scattering and absorption of anti-EGFR antibody conjugated gold nanoparticles in cancer diagnostics: applications in oral cancer. Nano Lett 2005; 5: 829–34.

[31] Kumar S, Harrison N, Richards-Kortum R, Sokolov K. Plasmonic nanosensors for

imaging intracellular biomarkers in live cells. Nano Lett 2007; 7: 1338–43.

[32] Park H, Lee SY, Chen L, Lee EK, Shin SY, Lee YH, et al. SERS imaging of HER2-overexpressed MCF7 cells using antibody-conjugated gold nanorods. Phys Chem Chem Phys 2009; 11: 7348–49.

[33] Singh R, Lillard JW. Nanoparticle-based targeted drug delivery. Exp Mol Pathol 2009; 86: 215–23.

[34] Kondoh M, Araragi S, Sato K, Higashimoto M, Takiguchi M, Sato M. Cadmium induces apoptosis partly via caspase-9 activation in HL-60 cells. Toxicology 2002; 170: 111–7.

[35] Yang L, Mao H, Wang YA, Cao Z, Peng X, Wang X, et al. Single chain epidermal growth factor receptor antibody conjugated nanoparticles for in vivo tumor targeting and imaging. Small 2009; 5: 235–43.

[36] Li Y, Schluesener HJ, Xu S. Gold nanoparticle-based biosensors. Gold bulletin 2010; 43: 29–41.

[37] Wu Z, Wu ZK, Tang H, Tang LJ, Jiang JH. Activity-based DNA-gold nanoparticle probe as colorimetric biosensor for DNA methyltransferase/glycosylase assay. Anal Chem 2013; 85: 4376−83.

[38] Springer T, Homola J. Biofunctionalized gold nanoparticles for SPR-biosensor-based detection of CEA in blood plasma. Anal Bioanal Chem 2012; 404: 2869–75.

[39] Qian X, Peng XH, Ansari DO, Yin-Goen Q, Chen GZ, Shin DM, et al. In vivo tumor targeting and spectroscopic detection with surface-enhanced raman nanoparticle tags. Nat Biotechnol 2008; 26: 83–90.

[40] Lee H, Lee K, Kim IK, Park TG. Synthesis, characterization, and in vivo diagnostic applications of hyaluronic acid immobilized gold nanoprobes. Biomaterials 2008; 29:

4709–18.

[41] Lee S, Cha EJ, Park K, Lee S, Hong J, Sun I, et al. A Near-infrared-fluorescence-quenched gold-nanoparticle imaging probe for in vivo drug screening and protease activity. Angew Chem 2008; 47: 2804–07.

[42] Cheng Y, Samia AC, Meyers HD, Panagopoulos I, Fei B, Burda C. Highly efficient drug delivery with gold nanoparticle vectors for in vivo photodynamic therapy of cancer. J Am Chem Soc 2008; 130: 10643–47.

[43] Park H, Tsutsumi H, Mihara H. Cell penetration and cell-selective drug delivery using α-helix peptides conjugated with gold nanoparticles. Biomaterials 2013; 34: 4872–9.

[44] You J, Zhang G, Li C. Exceptionally high payload of doxorubicin in hollow gold nanospheres for near-infrared light-triggered drug release. ACS Nano 2010; 4: 1033–41.

[45] Kojima C, Kono K, Maruyama K, Takagishi T. Synthesis of polyamidoamine dendrimers having poly(ethylene glycol) grafts and their ability to encapsulate anticancer drugs. Bioconjug Chem 2000; 11: 910–7.

[46] Kono K, Kojima C, Hayashi N, Nishisaka E, Kiura K, Watarai S, et al. Preparation and cytotoxic activity of poly(ethylene glycol)-modified poly(amidoamine) dendrimers bearing adriamycin. Biomaterials 2008; 29: 1664–75.

[47] Wang F, Wang YC, Dou S, Xiong MH, Sun TM, Wang J. Doxorubicin-tethered responsive gold nanoparticles facilitate intracellular drug delivery for overcoming multidrug resistance in cancer cells. ACS Nano 2011; 5: 3679–92.

Chapter 2.

Construction of α-helix peptide-conjugated gold nanospheres

2-1 Introduction

Much attention has recently been given to the development of intracellular drug delivery systems, which hold promising applications for human disease care. Carrier-based intracellular delivery has been investigated using various systems such as viral vectors [1], such as the retrovirus, lentivirus, herpes simplex virus and adenovirus, and non-viral vectors [2], such as liposome, cationic polymers and cell penetrating peptides (CPPs). Among these techniques, CPPs based intracellular delivery has several advantages such as the ease of synthesis or possibility of sequences modification.

On the other hands, gold nanospheres (GNSs) are the most studied nanomaterials in field of biological application research such as molecular imaging, biosensing, and in vivo studies, because they have advantages such as biocompatibility, high solubility, and physical properties such as strong absorption and scattering [3-8].

Mihara group constructed an α-helix peptide library, and 5-(and-6)-carboxytetramethylrhodamine (TAMRA dye) conjugated CPPs showed different CP activity against four cell lines (Figure 2-1), although some of these peptides had only one amino acid difference among 16 amino acids [9-12]. The α-helix peptides nanoprobes were constructed using four size of GNSs and two sequences of α-helix peptides selected from the peptide library. In addition, the peptide binding ability was evaluated according to size and their cytotoxicity.

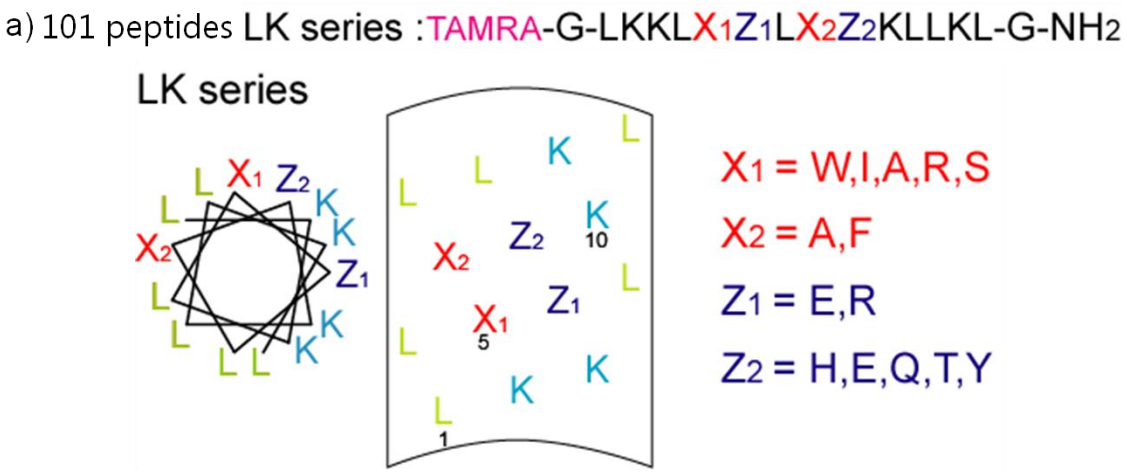

Figure 2-1 α-helix peptide library. Designed peptides in which four residues (X_1, Z_1, X_2, and Z_2) in the central region were replaced with other amino acids [9-12].

2-2 Materials and methods

2-2-1 Materials

Amino acids and reagents for peptide synthesis were purchased from Watanabe Chemical, Kokusan chemical and Hipep laboratories. Gold (III) chloride trihydrate was obtained from Sigma-Aldrich. Trisodium citrate dihydrate was obtained from Koso Chemical. PEG 2000 (Mw 2000) was purchased from Nof corporation.

2-2-2 Synthesis and purification of peptides

The peptides were synthesized by the conventional solid phase method using 9-fluorenylmethyloxycarbonyl (Fmoc) strategy [13]. The peptide chains were assembled on TGR resin using Fmoc amino acid derivatives (3 equiv), N,N-diisopropylethylamine (DIEA, 6 equiv), O-Benzotriazole-N,N,N',N'-tetramethyl-uronium-hexafluorophosphate (HBTU, 3 equiv), N-hydroxybenzotriazole (HOBt, 3 equiv) in N-methylpyrrolidone (NMP) for coupling, and 20% piperidine (PPD)/NMP for Fmoc removal. To cleave the peptide from the resin and remove the side chain protecting groups, the peptide resin was treated with trifluoroacetic acid (TFA) / m-cresol / thioanisole / ethandithiol (10 mL / 0.25 mL / 0.75 mL / 0.75 mL). All peptides were purified by reverse-phase HPLC on a Cosmosil 5C18-ARII packed column (10 × 250 mm) by using a linear gradient of acetonitrile / 0.1% TFA at a flow rate of 3.0 mL/min. The peptides were identified satisfactorily by matrix-assisted laser desorption ionization time-of-flight mass spectrometry (MALDI TOF-MS). MALDI TOF-MS was performed on a Shimadzu KOMPACT MALDI III mass spectrometer by using 3,5-dimethoxy-4-hydroxycinnamic acid as a matrix: Peptide EF (N), *m/z* obsd [M+H]+ 1911.5, *m/z* calcd [M+H]+ 1911.5; Peptide EF, *m/z* obsd [M+H]+ 1911.6, *m/z* calcd [M+H]+ 1911.5; Peptide EA (N), *m/z* obsd [M+H]+ 1835.2, *m/z* calcd

[M+H]+ 1835.4; Peptide EA, *m/z* obsd [M+H]+ 1835.5, *m/z* calcd [M+H]+ 1835.4. Full sequences of peptides are shown in Table 2-1, and named according to the Cys position: at C-terminus EF peptide: EF, at C-terminus EA peptide: EA, at N-terminus EF peptide: EF (N), at N-terminus EA peptide: EA (N).

Table 2-1. Peptides sequences

Name	Sequences
EF	GLKKLA**E**L**F**HKLLKLGC-NH_2
EA	GLKKLA**E**L**A**HKLLKLGC-NH_2
EF(N)	CGLKKLA**E**L**F**HKLLKLG-NH_2
EA(N)	CGLKKLA**E**L**A**HKLLKLG-NH_2

2-2-3 Synthesis of Gold nanospheres (GNS)

GNS was synthesized according to the Frens method [14] and scheme of GNS synthesis shows in Figure 2-2. After 50 mL of 0.01% gold (III) chloride trihydrate solution was started for boiling under reflux condition, added was 1.6 mL for 10 nm of GNS (GNS10), 1.0 mL for 16 nm (GNS16), 0.75 mL for 25 nm (GNS25), 0.5 mL for 41 nm (GNS41) of 1% trisodium citrate dehydrate solution as reducing agents. At this time, solution color was changed from yellow to colorless and then to red. The mixture was boiled for 20 min after color change and the heating was stopped. The diameter of the GNS was adjusted by volume of the trisodium citrate dehydrate, and characterized by UV-VIS spectroscopy (Shimadzu UV-2550 spectrometer) and transmission electron microscopy (TEM, Hitachi H-7500 electron microscope).

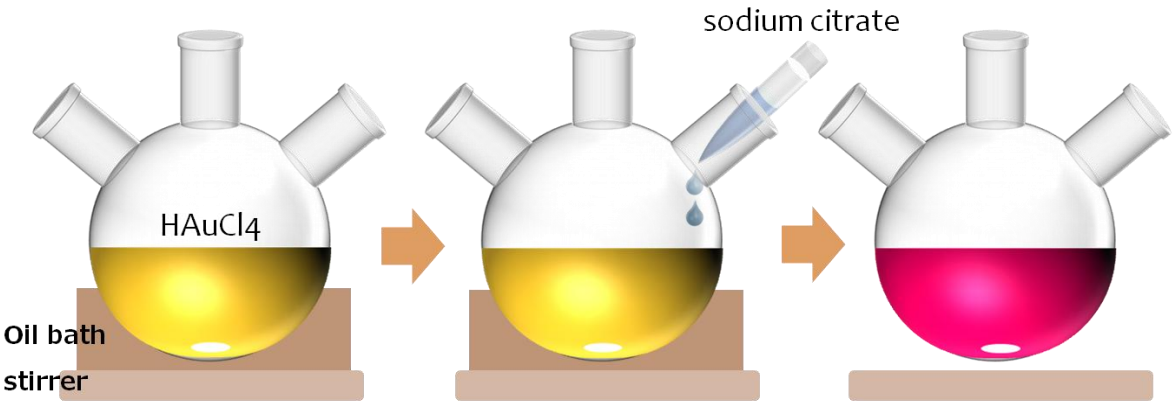

Figure 2-2. Scheme of gold nanospheres (GNS) synthesis

2-2-4 Conjugation of peptides (P-GNS) and PEG (PEG-GNS) with GNS

Various concentrations of EF and EA peptides were added to 1 mL of four kinds of GNSs [15]: 7 nM of GNS10, 3.4 nM of GNS16, 0.5 nM of GNS25, and 0.1 nM of GNS41 to check the peptide binding property. Then, the mixture was shaken on room temperature for 1 h, and washed by centrifugation at 9,000 rpm for 7 min with milli-Q water. Peptide-conjugated GNS (P-GNS) samples were characterized by UV-VIS spectroscopy.

2-2-5 Cytotoxicity of peptide-conjugated GNS41 (P-GNS41)

HeLa cells (human cervical cancer cell) $5x10^3$ in 100 μL of Dulbecco's modified eagle medium (DMEM) with 10% fetal bovine serum (FBS) and 1% penicillin-streptomycin (PS) were incubated in 96 well plate for 24 h at 37℃ under 5% CO_2. After washing 3 times with OPTI-MEM, 100 μL P-GNS samples (GNS only, 25 nM peptide EF (EF-GNS), peptide EA (EA-GNS), and PEG (PEG-GNS) were added. They were incubated for 2 h at 37℃ under 5% CO_2. After washing 3 times with OPTI-MEM, 10 μL of cell counting kit 8 (CCK-8) was added, and the mixture was incubated for 1 h at 37℃ under 5% CO_2. The absorption intensity was detected using a plate reader (ARVO MX 1420 multilabel counter, Perkin Elmer) at 450 nm, and the cell viability was calculated as 100 % cells viability of OPTI-MEM.

2-3 Results and Discussion

2-3-1 Characterization of GNS

10 nm, 16 nm, 25 nm, and 41 nm GNSs were synthesized according to Frens method [14]. They were characterized by UV-VIS spectroscopy (Shimadzu UV-2550 spectrometer) and transmission electron microscopy (TEM, Hitachi H-7500 electron microscope). Figure 2-3a shows the surface plasmon absorption spectra of 10 nm (GNS10): 518 nm, 16 nm (GNS16): 520 nm, 25 nm (GNS25): 525 nm, 41 nm GNS (GNS41): 530 nm, which was shifted according to increasing the GNS size. This result was corresponded with previous report [15]. Figure 2-3b)~e) shows the TEM images of GNS10, GNS16, GNS25, and GNS41.

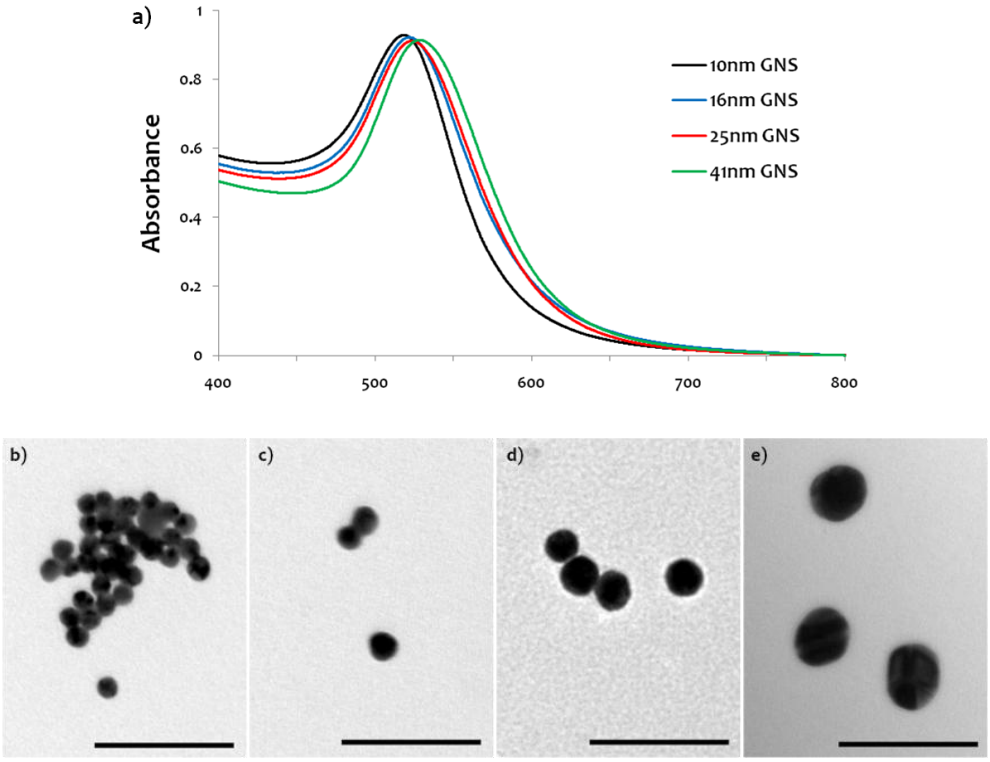

Figure 2-3 a) Surface plasmon absorption spectra of GNS black: 10 nm, blue : 16 nm, red : 25 nm, green : 41 nm. TEM images of GNSs: b) 10 nm, c) 16 nm, d) 25 nm, e) 41 nm. Scale bar: 100 nm.

2-3-2 Peptide conjugation with GNS

Using two peptide sequences, a Cys residue was used at C- or N-terminus of EF and EA peptide. These peptides were conjugated to GNS through a bond between the thiol of Cys and gold. After conjugation, four sizes of GNSs (10, 16, 25, and 41 nm) were investigated and examined in their ability to conjugate with peptides varying concentrations of peptides EF and EA (Figure 2-4). Among the four kinds of GNS, the GNS41 was selected, because it can conjugate with the largest amount of peptide per particle and afford a stronger light scattering property than the other GNS sizes. GNS10: 100-fold higher amount of peptide to GNS (7 nM) [Figure 2-4 (a) and (b)], GNS16: about 120-fold higher amount of peptide to GNS (3.4 nM) [Figure 2-4 (c) and (d)], GNS25: 500-fold higher amount of peptide to GNS (0.5 nM) [Figure 2-4 (e) and (f)] were completely aggregated and precipitated. In contrast, GNS41 showed the higher conjugation ability than GNS10, GNS16, and GNS25. By increasing the peptide concentration, the absorption intensity of GNS41 at 530 nm decreased, and a new peak appeared around 680 nm, indicating that the peptide conjugated GNS (P-GNS) aggregated with increasing peptide concentration [Figure 2-4 (g) and (h)]. The peak around 680 nm started increasing from as little as 5 nM of peptide conjugated to GNS41, and the absorbance was no longer observed at 200 nM of peptide conjugated to GNS41 because of complete aggregation and precipitation. At this concentration, there was 2000-fold higher amount of peptide to GNS (0.1 nM). As a results, 25 nM of peptide was used to conjugate GNS41 for further experiments, because it was the highest peptide concentration with the high stability for several months.

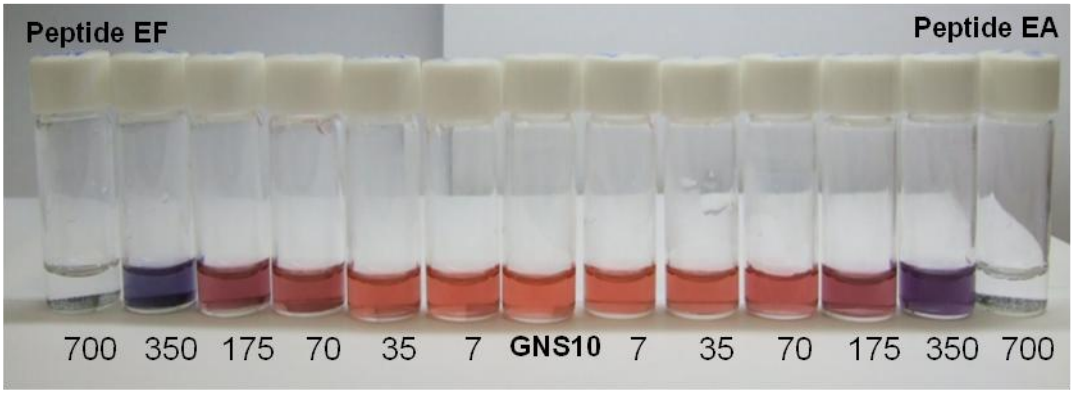
Peptide EF
Peptide EA
700 350 175 70 35 7 GNS10 7 35 70 175 350 700

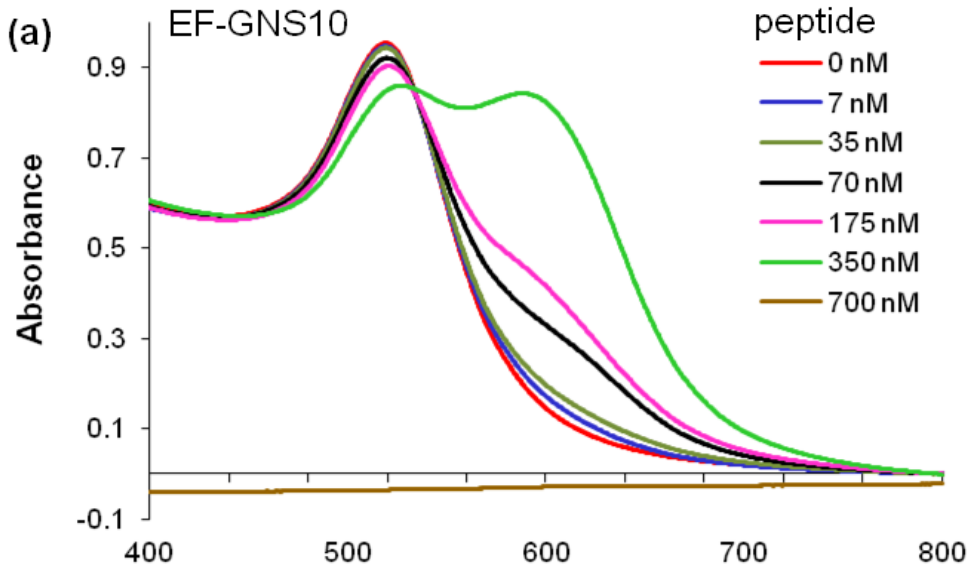
(a)
EF-GNS10
peptide
0 nM
7 nM
35 nM
70 nM
175 nM
350 nM
700 nM
Absorbance
0.9
0.7
0.5
0.3
0.1
-0.1
400
500
600
700
800

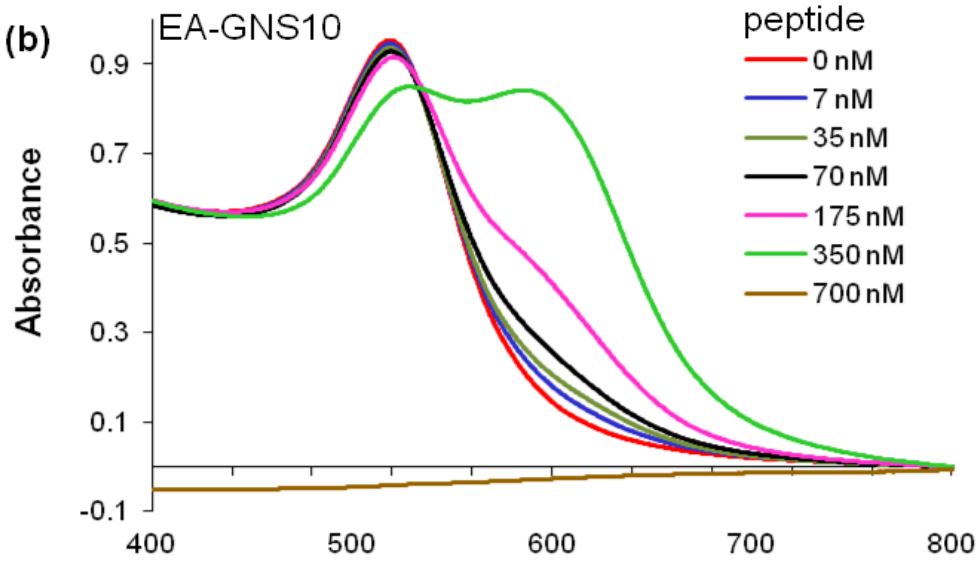
(b)
EA-GNS10
peptide
0 nM
7 nM
35 nM
70 nM
175 nM
350 nM
700 nM
Absorbance
0.9
0.7
0.5
0.3
0.1
-0.1
400
500
600
700
800

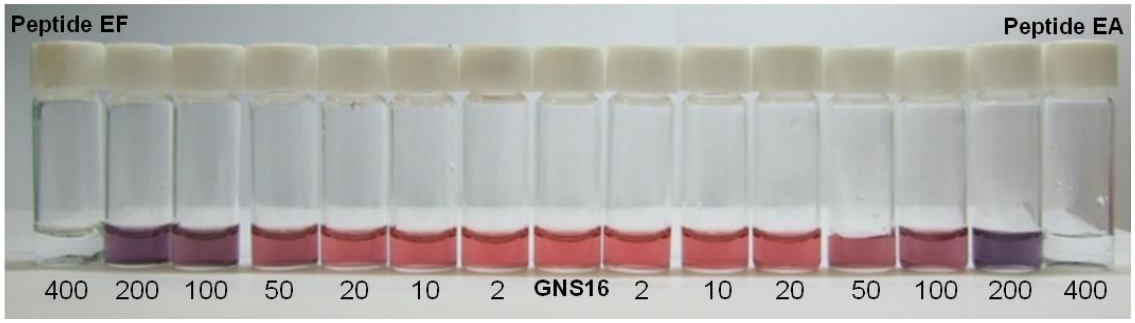
Peptide EF
Peptide EA
400 200 100 50 20 10 2 GNS16 2 10 20 50 100 200 400

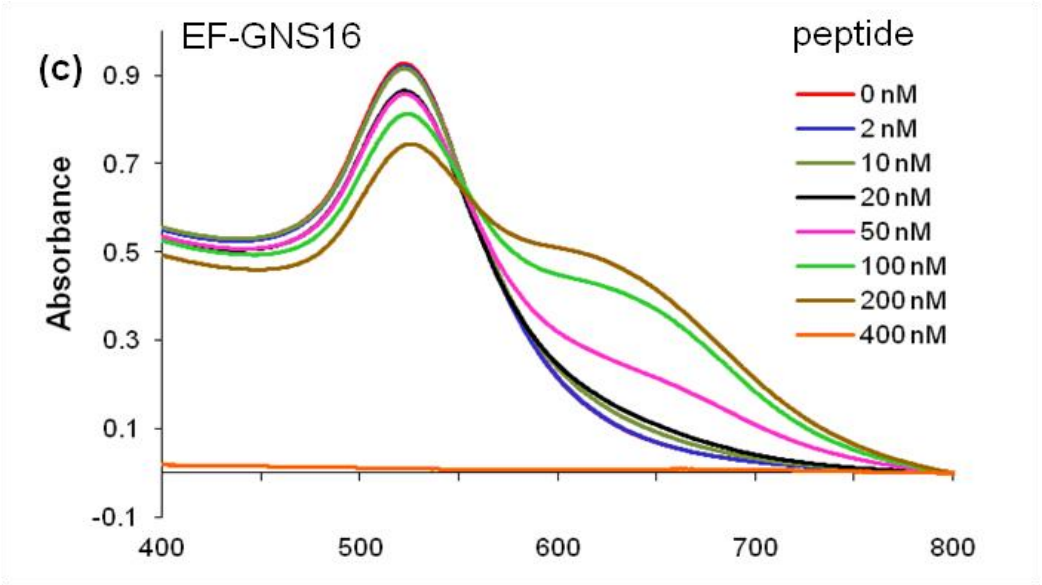
(c)
EF-GNS16
peptide
0 nM
2 nM
10 nM
20 nM
50 nM
100 nM
200 nM
400 nM
Absorbance
0.9
0.7
0.5
0.3
0.1
-0.1
400
500
600
700
800

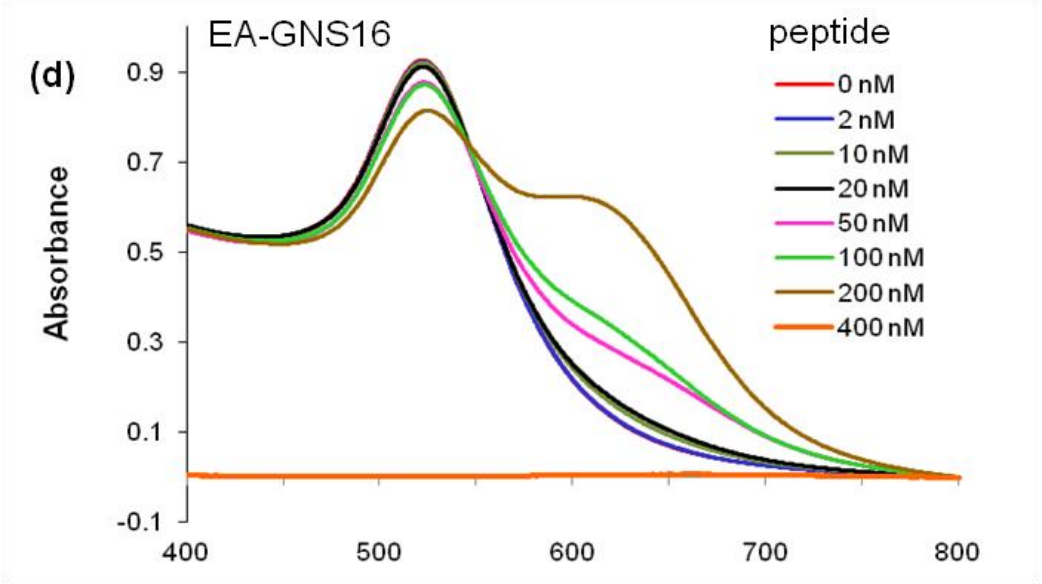
(d)
EA-GNS16
peptide
0 nM
2 nM
10 nM
20 nM
50 nM
100 nM
200 nM
400 nM
Absorbance
0.9
0.7
0.5
0.3
0.1
-0.1
400
500
600
700
800

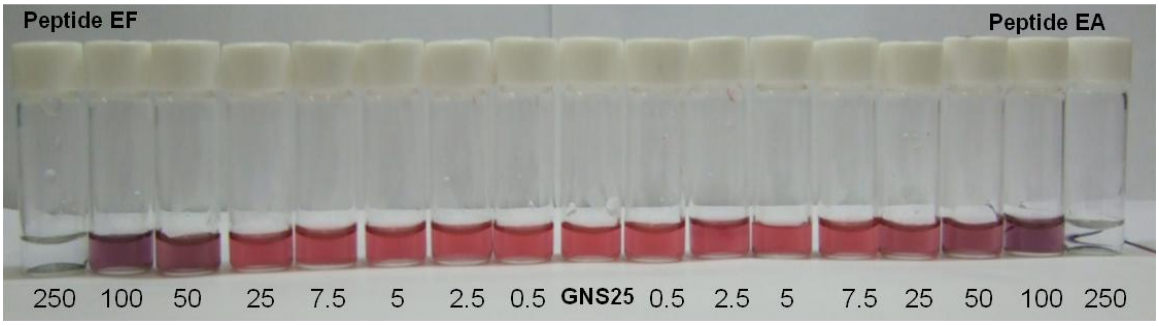
Peptide EF
Peptide EA
250 100 50 25 7.5 5 2.5 0.5 GNS25 0.5 2.5 5 7.5 25 50 100 250

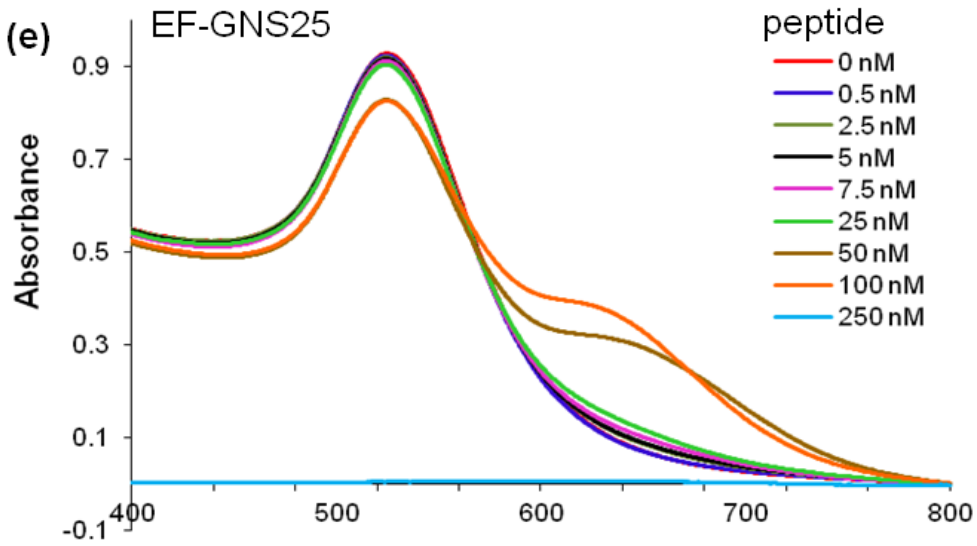
(e)
EF-GNS25
peptide
0 nM
0.5 nM
2.5 nM
5 nM
7.5 nM
25 nM
50 nM
100 nM
250 nM
Absorbance
0.9
0.7
0.5
0.3
0.1
-0.1
400
500
600
700
800

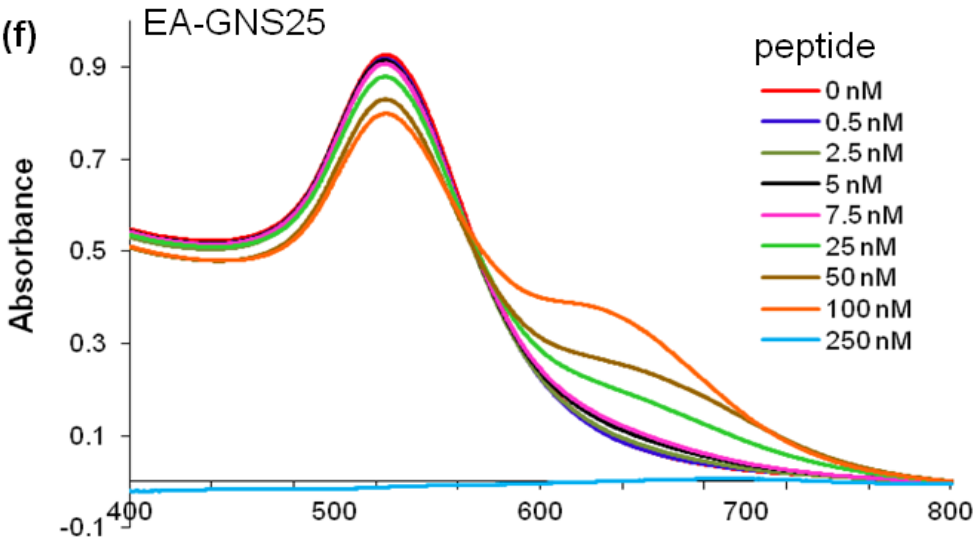
(f)
EA-GNS25
peptide
0 nM
0.5 nM
2.5 nM
5 nM
7.5 nM
25 nM
50 nM
100 nM
250 nM
Absorbance
0.9
0.7
0.5
0.3
0.1
-0.1
400
500
600
700
800

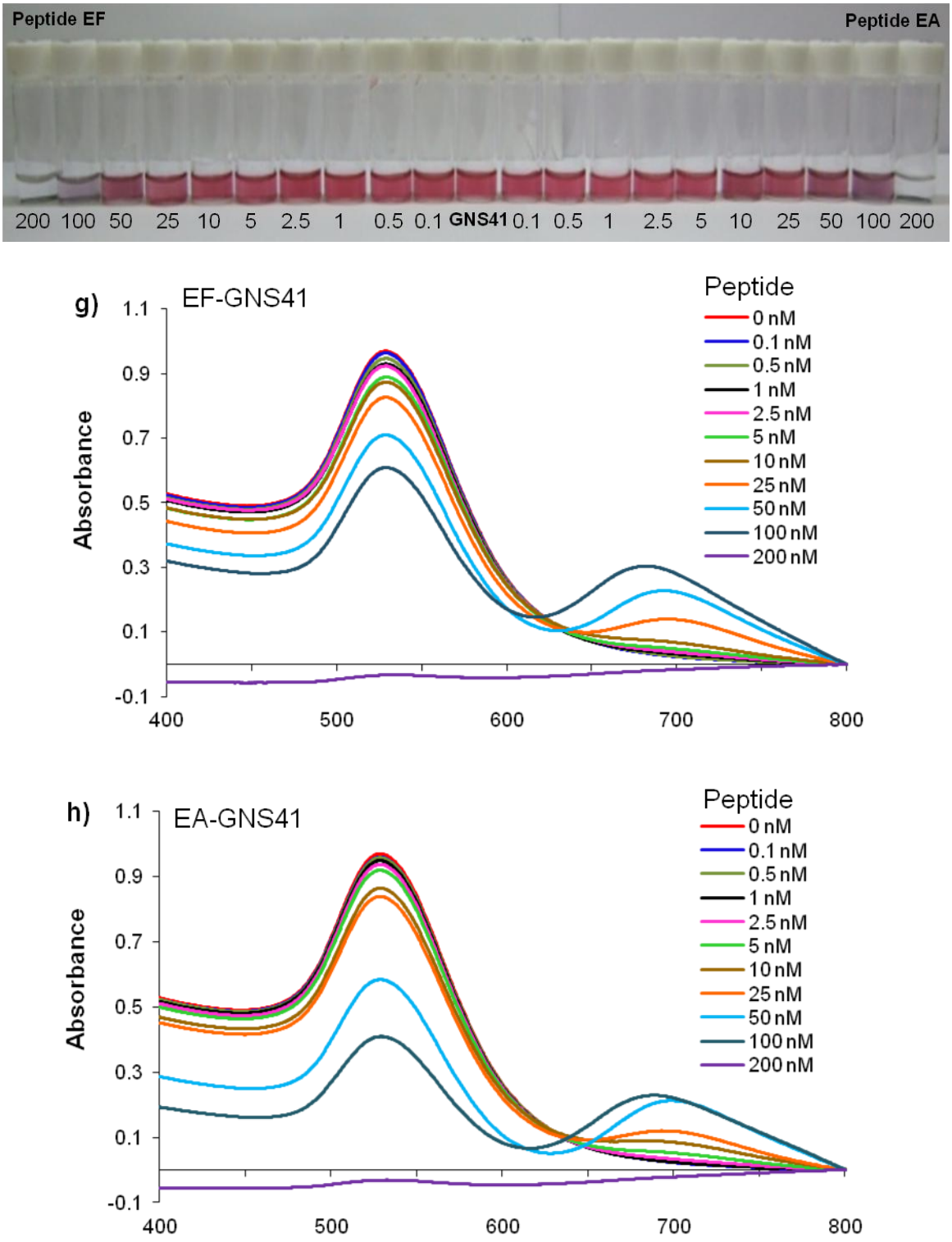

Figure 2-4 Surface plasmon absorption spectra and photos (number of bottom: peptide concentrarion: nM) of a), b) GNS10, c), d) GNS16, e), f) GNS25, and, g), h) GNS41 according to increase of the concentration peptide EF (a, c, e, g) and peptide EA (b, d, f, h).

2-3-3 Cytotoxicity of GNS41, PEG-GNS41, and P-GNS41.

The cytotoxicity of GNS41 and P-GNS41 was evaluated using CCK-8 against HeLa cell. PEG-GNS41 was used to compare the cytotoxicity with P-GNS41. GNS41 was conjugated with 25 nM peptides EF and EA, and PEG (Mw 2000) for 1 h at room temperature. The GNS, PEG-GNS41, EF-GNS41, and EA-GNS41 complexes were incubated with HeLa cells for 2 h, and the absorption intensity at 450 nm was measured using a plate reader. Figure 2-5 shows the cell viability of GNS41, PEG-GNS41, EF-GNS41, and EA-GNS41 against HeLa cell. GNS41, EF-GNS41, and EA-GNS41 showed over 90% cell viabilities, which were similar to the values of PEG-GNS. PEG is a nontoxic material used for pharmaceuticals and drug delivery researches and also with gold nanoparticles [16,17]. Cell viability was calculated as the viability of OPTI-MEM was 100%. These results demonstrated that all the GNS41 complexes did not have high cytotoxicity.

.

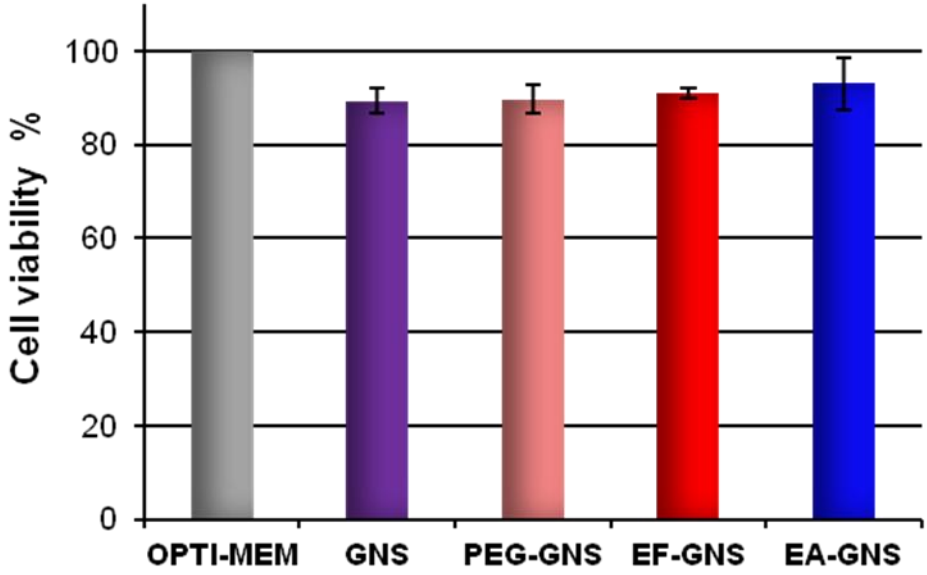

Figure 2-5 In vitro cytotoxicity test of GNS41, PEG (25 nM) conjugated GNS41 (PEG-GNS41) and peptides EF and EA (25 nM) conjugated GNS41 (EF-GNS41, EA-GNS41) against HeLa cell.

2-4 Conclusions

In this study, the four kinds of α-helix peptides nanoprobes was constructed and evaluated their peptide binding ability according to GNS size (10, 16, 25, 41 nm). Among them, GNS41 conjugated the largest amount of peptide per particle and showed the low cytotoxicity against HeLa cell. The constructed α-helix peptides nanoprobes have the potential to molecular imaging and delivery system with high biocompatibility and bioconjugation ability on GNS surface. These functions will be demonstrated in the following chapters.

Reference

[1] Thomas CE, Ehrhardt A, Kay MA. Progress and problems with the use of viral vectors for gene therapy. Nat rev Genet 2003; 4: 346–58.

[2] Niidome T, Huang L. Gene therapy progress and prospects: Nonviral vectors. Gene Ther 2002; 9: 1647–52.

[3] El-Sayed IH, Huang X, El-Sayed MA. Surface plasmon resonance scattering and absorption of anti-EGFR antibody conjugated gold nanoparticles in cancer diagnostics: applications in oral cancer. Nano Lett 2005; 5: 829-34.

[4] Kumar S, Harrison N, Richards-Kortum R, Sokolov K. Plasmonic nanosensors for imaging intracellular biomarkers in live cells. Nano Lett 2007; 7: 1338–43.

[5] Song S, Qin Y, He Y, Huang Q, Fan C, Chen H.Y. Functional nanoprobes for ultrasensitive detection of biomolecules. Chem Soc Rev 2010; 39: 4234–43.

[6] Qian X, Peng XH, Ansari DO, Yin-Goen Q, Chen GZ, Shin DM. et al. In vivo tumor targeting and spectroscopic detection with surface-enhanced raman nanoparticle tags. Nat Biotechnol 2008; 26: 83–90.

[7] Cheng Y, Samia AC, Meyers JD, Panagopoulos I, Fei B, Burda C. Highly efficient drug delivery with gold nanoparticle vectors for in vivo photodynamic therapy of cancer. J Am Chem Soc 2008; 130: 10643–7.

[8] Medley CD, Smith JE, Tang Z, Wu Y, Bamrungsap S, Tan W. Gold nanoparticle-based colorimetric assay for the direct detection of cancerous cells. Anal Chem 2008; 80: 1067-72.

[9] Usui K, Tomozaki K, Mihara H. Protein-fingerprint data mining of a designed α-helical peptide array. Mol BioSyst 2006; 2: 417-20.

[10] Usui K, Tomozaki K, Mihara H. Screening of α-helical peptide ligands controlling a

calcineurin-phosphatase activity. Bioorg Med Chem Lett 2007; 17: 167-71.

[11] Usui K, Kakiyama T, Tomozaki K, Mie M, Kobatake E, Mihara H. Cell fingerprint patterns using designed α-helical peptides to screen for cell-specific toxicity. Bioorg Med Chem Lett 2011; 21: 6281-4.

[12] Usui K, Kikuchi T, Mie M, Kobatake E, Mihara H. Systematic screening of the cellular penetration of designed alpha-helix peptides. Bioorg. Med. Chem. 2013; 21: 2560-7.

[13] Chan WC, White PD. Eds. Fmoc solid phase peptide synthesis. New York: Oxford University Press 200041-76.

[14] G Frens. Controlled nucleation for the regulation of the particle size in monodisperse gold suspensions. Nat Phys Sci 1973; 241: 20–2.

[15] Ghosh SK, Pal A, Kundu S, Nath S, Pal T. Fluorescence quenching of 1-methylaminopyrene near gold nanoparticles: size regime dependence of the small metallic particles. Chem Physics Lett 2004; 395: 366–72.

[16] Niidome T, Yamagata M, Okamoto Y, Akiyama Y, Takahashi H, Kawano T, et al. PEG-modified gold nanorods with a stealth character for in vivo applications. J Control Release 2006; 114: 343–7.

[17] Veronese FM, Pasut G. PEGylation, successful approach to drug delivery. DDT 2005; 10: 1451–58.

Chapter 3.

Cell penetrating activity and drug delivery application of α-helix peptide-conjugated gold nanospheres

3-1 Introduction

Cell penetrating peptides (CPPs)-based intracellular delivery has several advantages, such as the ease of synthesis or possibility of sequences modification [1-7]. Although typical CPPs such as TAT show the high cell penetrating (CP) activity, the peptide has a low cell selectivity, which is an important factor especially cancer therapy application. However, TAMRA (5-(and-6)-carboxytetramethylrhodamine) conjugated CPPs of a 16-amino acid peptide library from Mihara group [8-11] showed different CP activity against four cell lines, although some of these peptides had only one amino acid difference among 16 amino acids [11].

In this study, four kinds of nanoprobes using EF and EA peptide conjugated gold nanospheres (P-GNS) were constructed (Figure 3-1a) and examined their cytotoxicity and peptide binding property GNSs with various sizes in chapter 2. GNS [12-15] would function as an imaging agent with multi-peptide conjugation for cell interactions and are applicable to drug delivery by conjugation of an anti-cancer drug on the GNS surface.

In chapter 3, the CP activity and drug delivery applicability of peptide-conjugated 41 nm GNS (P-GNS41) were described because they showed the high binding ability on GNS41 compared to other GNSs (GNS10, GNS16, and GNS25). Furthermore, the applicability of P-GNSs41 to drug delivery in three cell lines were examined by conjugati ng anti cancer drug, doxorubicin (DOX), which is an anti-cancer drug that intercalates with DNA and inhibits macromolecular biosynthesis, onto the GNS41 surface (P-DOX-GNS41) [16].

3-2 Materials and methods

3-2-1 Materials

Penicillin-streptomycin (PS) was obtained from Sigma-Aldrich. PEG 2000 (Mw 2000) was purchased from Nof corporation. Dulbecco's modified eagle's medium (DMEM) was obtained from Wako Pure Chemicals. OPTI-MEM was obtained from Gibco. Cell counting kit-8 (CCK-8) was purchased from Dojindo Molecular Technologies.

3-2-2 Cell internalization of P-GNS41 for three kinds of cells

HeLa cells and A549 cells were cultured in DMEM supplemented with 10% FBS and 1% PS, and 3T3-L1 cells were cultured in DMEM supplemented with 10% Donor Bovine Serum (DBS) and 1% PS to prevent the cell differentiation at 37℃ under 5% CO_2. For cell labeling, $5x10^4$ cells were placed on 22x22 mm cover slip in 6 well cell culture plates and cultured overnight at 37℃ under 5% CO_2. After washing twice with OPTI-MEM, 200 μL of GNS41 only, PEG-GNS41, EF-GNS41, EA-GNS41, EF(N)-GNS41 and EA(N)-GNS41 (25 nM peptide and PEG conjugated GNS41) were added in each plate and incubated for 2 h. They were washed twice with OPTI-MEM, coated with 90% glycerol and sealed to slide glass. Dark-field images based on elastic light scattering were taken using a Nikon microscope (Ti-U) with an immersion dark field condenser.

3-2-3 Construction of DOX conjugated with GNS41 (DOX-GNS41) and P-GNS41 (P-DOX-GNS41)

DOX 0.01-10 μM was mixed with 1 mL of 41 nm GNS (DOX-GNS41) for conjugation using electrostatic interaction between positive charge of DOX amino group

and negative charge of GNS surface [16], which is a weaker interaction than the covalent bond between peptide and GNS41. After 1 h shaking, they were centrifuged at 8,000 rpm for 8 min and washed with milli-Q water to remove unconjugated DOX. 10, 50, 100 nM DOX and peptide EF or EA 25 nM with GNS41 (P-DOX-GNS41) were shaken for 1 h at room temperature, and centrifuged at 8,000 rpm for 8 min.

3-2-4 Cell death activity of P-DOX-GNS41

DOX-GNS41 and P-DOX-GNS41 were prepared according to the described method in Chapter 3-2-3. HeLa and A549 ($5x10^3$ cells) in 100 μL of DMEM supplemented with 10% FBS and 1% PS and 3T3-L1 ($2x10^3$ cells) in 100 μL of DMEM plus 10% DBS and 1% PS were incubated in 96 well plate for 24 h at 37℃ under 5% CO_2. After washing 3 times with OPTI-MEM, 100 μL of the OPTI-MEM, GNS41 only, 10 nM to 10 μM DOX solution and DOX-GNS41, EF-DOX-GNS41, EA-DOX-GNS41 (25 nM peptide-GNS41 conjugation with 10, 50, and 100 nM DOX) were added. They were incubated for 2 h at 37℃ under 5 % CO_2. Cell plate was incubated for 24 h at 37℃ under 5% CO_2 for release of DOX after washing 3 times with OPTI-MEM. 10 μL of CCK-8 was added, and the mixture was incubated for 1 h at 37℃ under 5% CO_2. The absorption intensity was detected using the plate reader (ARVO MX 1420 multilabel counter, Perkin Elmer) at 450 nm, and the cell viability was calculated as 100% cells viability of OPTI-MEM.

(a)

Name	Sequences
TAMRA-EF	TAMRA-G-LKKLA**E**L**F**HKLLKLG-NH_2
TAMRA-EA	TAMRA-G-LKKLA**E**L**A**HKLLKLG-NH_2
EF-GNS41	GLKKLA**E**L**F**HKLLKLG-C-GNS
EA-GNS41	GLKKLA**E**L**A**HKLLKLGC-GNS
EF(N)-GNS41	GNS-CGLKKLA**E**L**F**HKLLKLG-NH_2
EA(N)-GNS41	GNS-CGLKKLA**E**L**A**HKLLKLG-NH_2

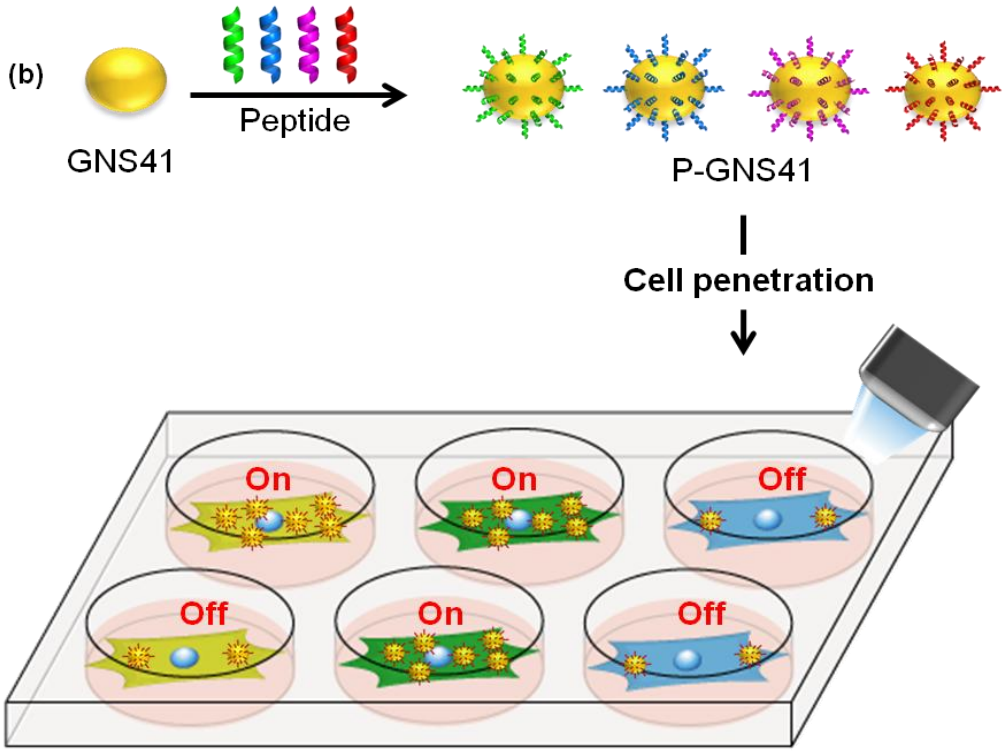

Figure 3-1 a) Sequences of original TAMRA-peptides EF and EA, and four GNS41 conjugated peptides EF-, EA-, EF(N)- and EA(N)-GNS, b) Scheme of peptides conjugation with GNS41, and cell penetration using peptide conjugated GNS41 (P-GNS41)

3-3 Result and Discussion

3-3-1 Dark field images of HeLa, A549 and 3T3-L1 cells after incubation with P-GNS41

Figure 3-1 shows a) the full sequences of EF-, EA-, EF(N)-, EA(N)-GNS41, and b) scheme of cell internalization P-GNS41. Cell internalization of nanoprobes were evaluated on (high CP activity) or off (low CP activity). The strong light scattering property of GNS due to the localized surface plasmon resonance, together with photostability, make GNS a powerful contrast agent for light scattering imaging. Figure 3-2 shows the bright and dark field light scattering images of HeLa, A549 and 3T3-L1 cells after incubation with GNS41, PEG-GNS41, EF-GNS41, EA-GNS41, EF(N)-GNS41 and EA(N)-GNS41. The HeLa cells showed no interaction with only GNS41. PEG-GNS41 attached to the cell membrane and showed low CP activity. EF-GNS41 showed high CP activity for HeLa cells, while EA-GNS41 and EA(N)-GNS41 attached the cell membrane and showed low CP activity. These results are comparable to those in the previous research with TAMRA conjugated peptide [11]. TAMRA conjugated EF showed high CP activity, and TAMRA conjugated EA showed low CP activity for HeLa cells. However, it is interesting that EF(N)-GNS41 showed low cellular internalization. EF-GNS41 and EF(N)-GNS41 had a large contrast in their CP activity, despite having the same peptide sequence and net charge. It was thought that they may arise the CP activity difference by the directivity from the peptide conjugating to GNS, this directivity make the different terminus groups of EF-GNS41 (amino) and EF(N)-GNS41 (amide). For A549 cells, GNS41 and PEG-GNS41 showed low CP activity; all P-GNSs (EF-GNS41, EF(N)-GNS41, EA-GNS41 and EA(N)-GNS41) displayed high CP activity. The direction of the peptide on the GNS did not change the activity with A549 cells. As TAMRA-EF and EA showed a similar CP activity (scored +++)

for A549 cells [11], P-GNS41 also had similar CP activity with EF-GNS41 and EA-GNS41. Low cell internalization was observed for all samples with 3T3-L1 cells. This result also corresponded with that of the TAMRA-peptides. Although peptides EF and EA have only one amino acid difference, they displayed different CP activity with different cell types; that is, EF-GNS41 with Phe had higher CP activity with both HeLa and A549 cells, while EA-GNS41 had high activity only for the A549 cells. It is also noteworthy that P-GNS41 could be used for the dark images with only 25 nM peptide, which is approximately 100 fold lower than the concentration used in previous research with a free TAMRA-peptide (2 μM). This result may be due to the effect of multi-peptide conjugation on GNS for the cell interaction. The CP mechanism of designed peptides is unclear now but they it will be useful tool for specific cell penetration clarifying mechanism between them and cell surface.

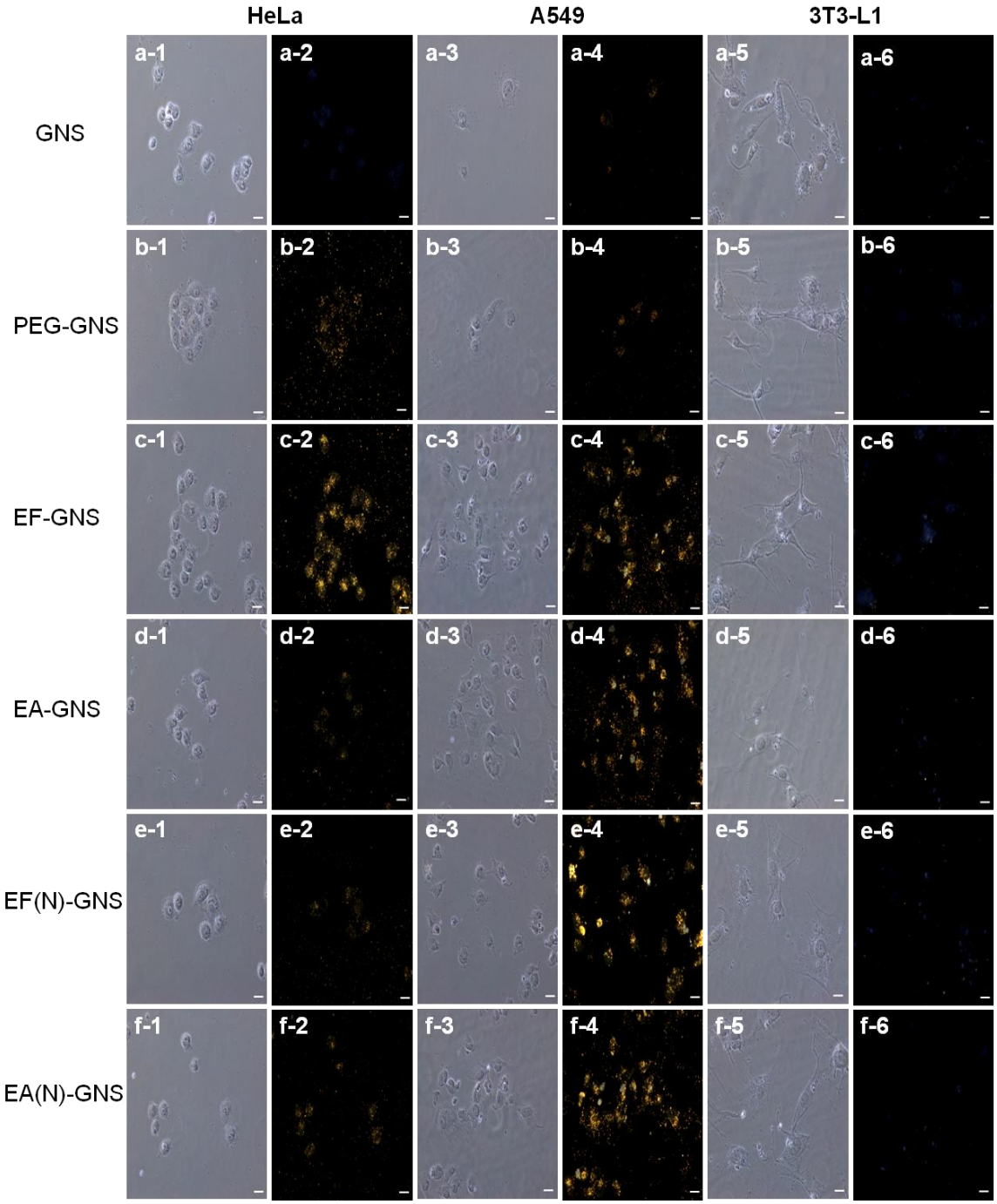

Figure 3-2 Bright field (1, 3, 5) and dark field light scattering images (2, 4, 6) of EF and EA. 1 and 2: HeLa, 3 and 4: A549, 5 and 6: 3T3-L1 cells. a: only GNS41, b: PEG-GNS41, c: EF-GNS41, d: EA- GNS41, e: EF(N)-GNS41, f: EA(N)-GNS41

3-3-2 Optimization of the conjugation condition of doxorubicin (DOX) with P-GNS41

In Figure 3-3a, 10 and 1.0 μM DOX-GNS41 aggregated after 1 h of reaction, while 0.1 μM DOX-GNS41 did not. 0.1 μM DOX afforded stable DOX-GNS41 and DOX-GNS41 with peptide conjugation (25 nM) P-DOX-GNS41. The samples were kept in stable for several months after washing by centrifugation.

Supernatant of P-DOX-GNS41 DOX-GNS41 samples after wash were transfered to microtube. They were conpared with free DOX solutions of same concentration. These solutions were analysed by the fluorescent emission intensity at 560 nm with 488 nm excitation to check the residual DOX amount using fluorescent intensity of DOX. DOX has the fluorescent signal from 550 nm to 620 nm with 488nm excitation. Figure 3-3b shows the fluorescence intensity of DOX solution, DOX-GNS41, EF-GNS41 and EA-GNS41 on the 3 kinds of DOX concentrations of 10, 50, 100 nM. The results of over 70 % decrease in fluorescence intensity verified the conjugation of DOX to GNS41 against free DOX solution. DOX were quantitatively conjugated to GNS41 surface also in the presence of peptides.

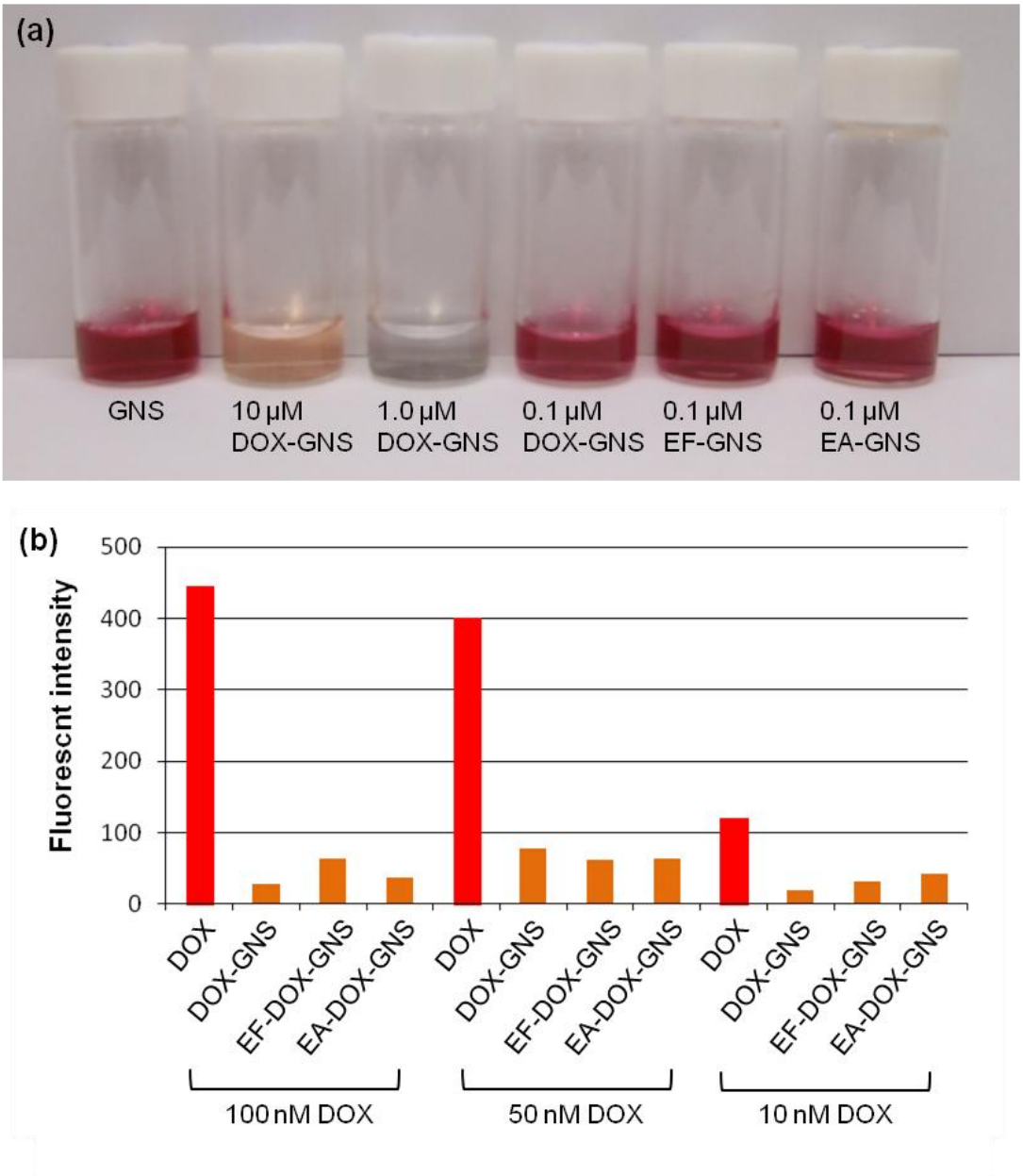

Figure 3-3 a) GNS41, 10 µM, 1.0 µM, 0.1µM DOX-GNS41 and 0.1 µM P-DOX-GNS41 samples after centrifugation b) Comparison of the fluorescent intensity of the upper solution of DOX-GNS41, EF-DOX-GNS41 and EA-DOX-GNS41 after centrifugation and free DOX solution in 3 different concentrations of DOX (100 nM, 50 nM, 10 nM).

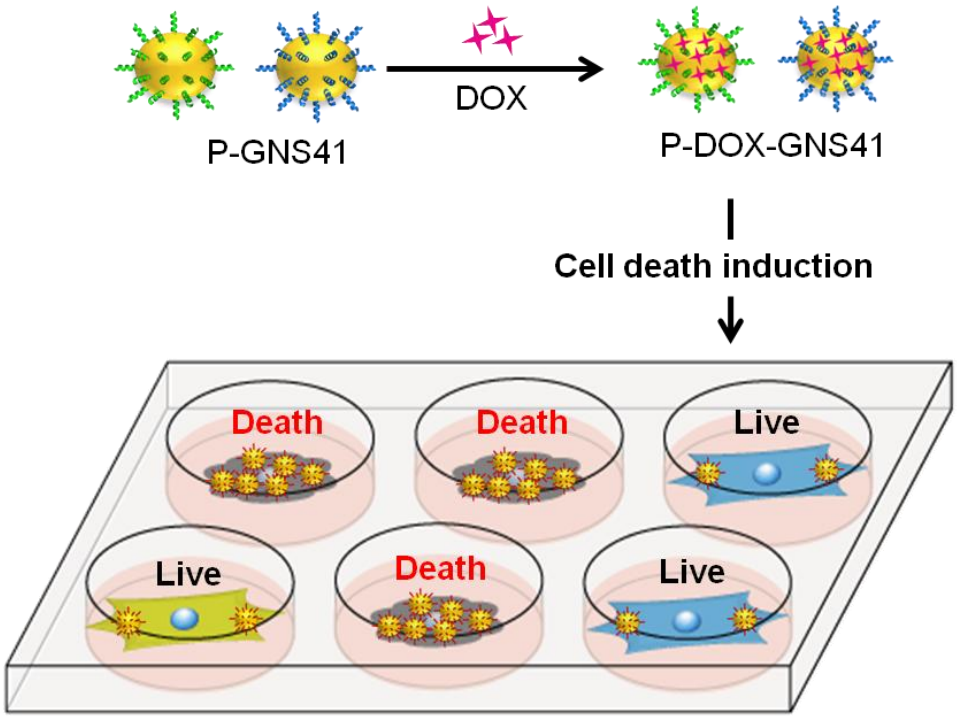

Figure 3-4 Scheme of peptides and DOX conjugation with GNS41, and cell penetration and cell death induction using peptide conjugated GNS41 (P-GNS41) and P-DOX-GNS41

3-3-3 Selective cytotoxicity of DOX conjugated P-GNS41

P-GNSs41 showed cell-selective penetrating activity with the three cell lines. DOX, an anticancer drug, was conjugated to GNS41 (DOX-GNS41) and P-GNS41 (EF-DOX-GNS and EA-DOX-GNS41), and the cell-selective drug delivery activity was determined using EF-DOX-GNS and EA-DOX-GNS with the three cell lines shown in illustration (Figure 3-4). Figure 3-5 shows the cell death induction activity of the DOX-conjugated complexes DOX-GNS41 (orange bar), EF-DOX-GNS41 (red bar) and EA-DOX-GNS41 (blue bar) with different concentrations (10, 50, and 100 nM) of DOX for the HeLa, A549 and 3T3-L1 cell lines. The green bar shows the cell viability of free DOX solution with increasing of concentration (10 nM-10 μM) and displays the decrease of cell viability in the three cell lines. In the HeLa cells (Figure 3-5a), free DOX solution (100 nM) had 53% cell viability, EF-DOX-GNS41 showed 41% cell viability, and EA-DOX-GNS41 and DOX-GNS41 showed 91% and 86% cell viability, respectively. The HeLa cells showed the same tendency at 50 nM (DOX solution: 67%, EF-DOX-GNS41: 53%) and 10 nM (DOX solution: 86%, EF-DOX-GNS: 76%). EF-DOX-GNS41 showed over 10% higher cell death activity than free DOX solution under the same conditions. Although it is thought that all physically adsorbed DOX molecules could not be completely liberated from GNS41, EF-DOX-GNS41 showed a higher activity. In contrast, DOX-GNS41 and EA-DOX-GNS41 indicated low cell death induction for the HeLa cells, with high cell viability of over 80%. In the A549 cell line (Figure 3-5b), both EF-DOX-GNS41 and EA-DOX-GNS41 showed cell death induction that was approximately 20% higher than the free DOX solution under the same conditions. DOX-GNS41 had low amounts of cell death induction at all concentrations. In the 3T3-L1 cell line (Figure 3-5c), all samples indicated low cell death induction values, with over 90% cell viability. The results of the cell death

induction assays corresponded with the results from the cell penetrating activity of EF-GNS and EA-GNS. The selective and higher cell death activity of P-DOX-GNSs41 could be attributed to the CP activity of the P-GNSs.

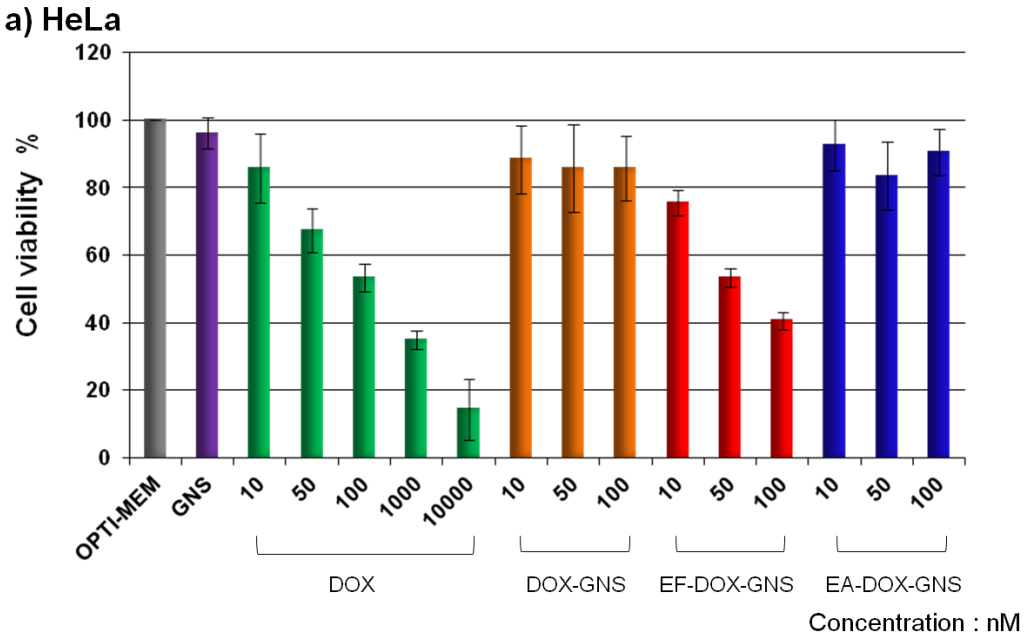
a) HeLa
Cell viability %
120
100
80
60
40
20
0
OPTI-MEM
GNS
10
50
100
1000
10000
10
50
100
10
50
100
10
50
100
DOX
DOX-GNS
EF-DOX-GNS
EA-DOX-GNS
Concentration : nM

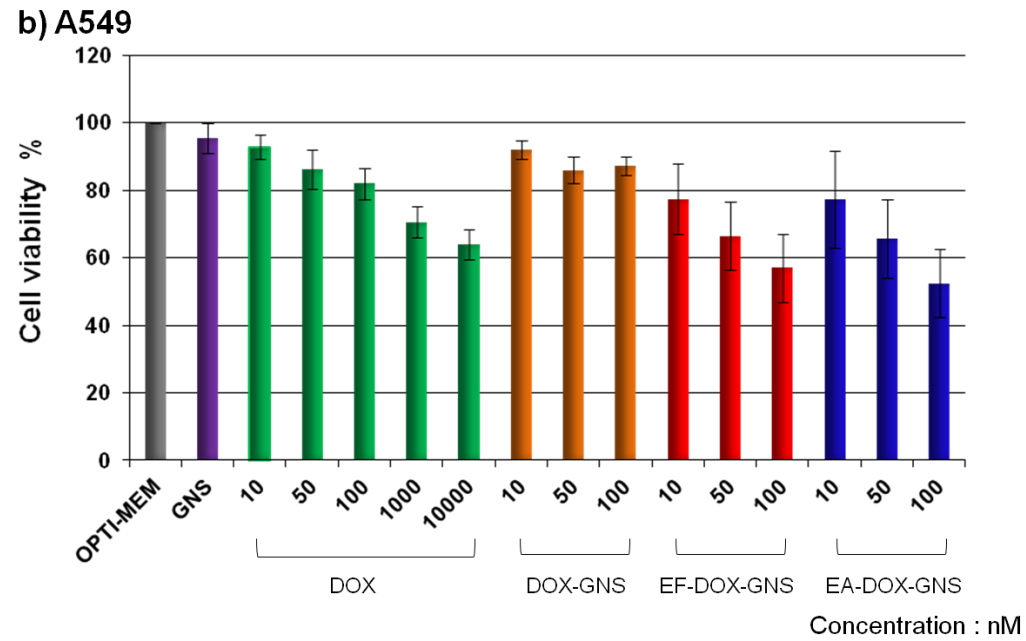
b) A549
Cell viability %
120
100
80
60
40
20
0
OPTI-MEM
GNS
10
50
100
1000
10000
10
50
100
10
50
100
10
50
100
DOX
DOX-GNS
EF-DOX-GNS
EA-DOX-GNS
Concentration : nM

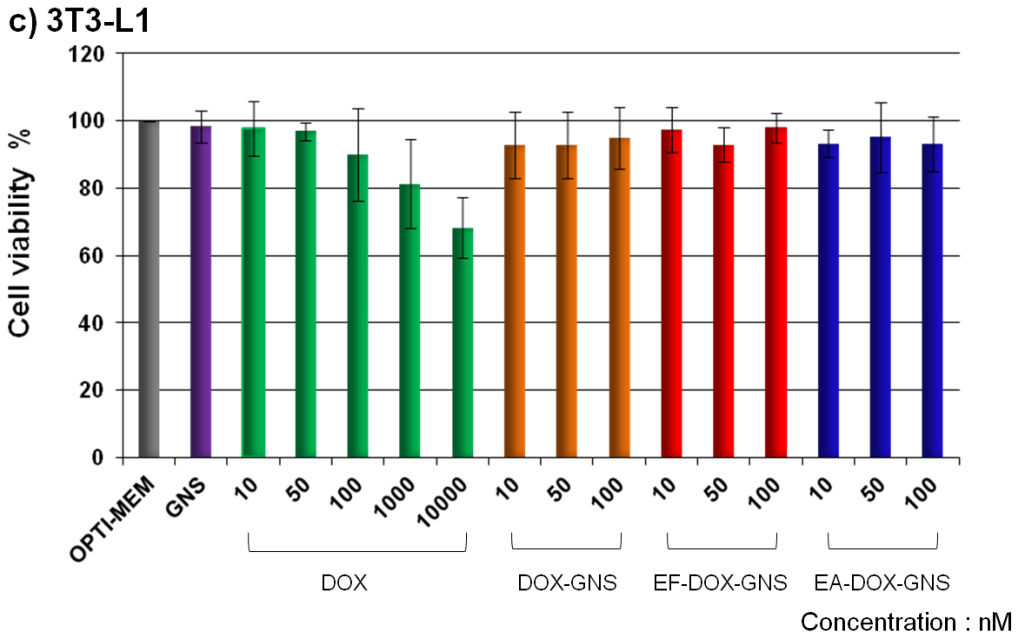

Figure 3-5 Cell death activity on (a) HeLa, (b) A549, (c) 3T3-L1 of free DOX solution, DOX-GNS41, DOX-EF-GNS41, DOX-EA-GNS41 on the 3 kinds of DOX concentrations of 10, 50, 100 nM. Grey bar : OPTI-MEM, violet bar : GNS41 only, green bar : free DOX solution, orange bar : DOX-GNS41, red bar : EF-DOX-GNS41, blue bar : EA-DOX-GNS41.

3-3-4 Dark field images of DOX conjugated complexes (P-DOX-GNS41)

To determine the cell internalization of the DOX conjugated complexes, DOX-GNS41, EF-DOX-GNS41 and EA-DOX-GNS41 were applied to HeLa, A549, and 3T3-L1 cells. Figure 3-6 shows the bright and dark field images of DOX-GNS41, EF-DOX-GNS41 and EA-DOX-GNS41. The cell labeling method was the same as that of the detection experiments in the dark field images of the P-GNS41 complexes. As shown in Figure 3-6, for the HeLa cell line, EF-DOX-GNS41 showed higher CP activity, but EA-DOX-GNS41 did not. In the A549 cell line, both EF-DOX-GNS41 and EA-DOX-GNS41 showed higher activity. For the 3T3-L1 cell line, high internalization was not observed. DOX-GNS41 showed low cell internalization for all cell lines. These results confirmed that the cell internalization properties of DOX conjugated P-GNSs41 were completely comparable to those of the P-GNSs41 (Figure 3-2) and the cell death activity (Figure 3-5). It was supposed that DOX conjugated non-covalently was liberated from GNS41 to function as the anticancer drug. The DOX activity for cell death was derived from the CP activity of the P-GNS41, indicating that P-GNSs41 have a cell-selective drug delivery function.

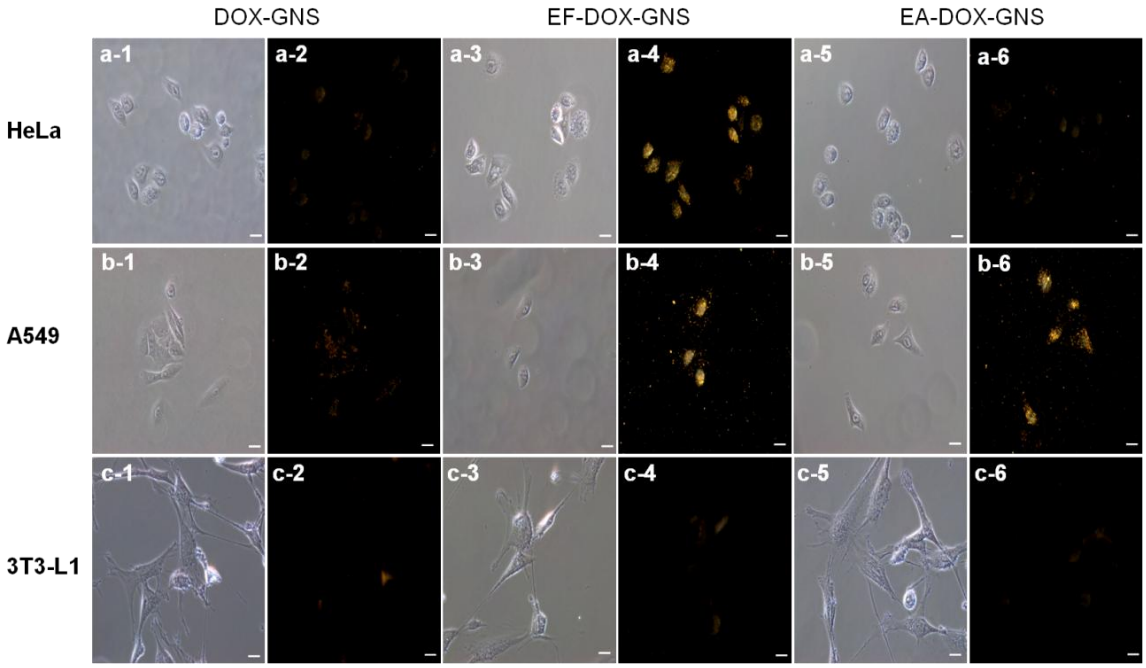

Figure 3-6 Bright field (1, 3, 5) and dark field light scattering images (2, 4, 6) of a) HeLa, b) A549, c) 3T3-L1, 1 and 2: DOX-GNS41, 3 and 4: EF-DOX-GNS41, 5 and 6: EA-DOX-GNS41

3-3-5 Dark field images of HeLa, A549 and 3T3-L1 cells after incubation with P-DOX-GNS41 in DMEM containing serum

The CP activity of EF-DOX-GNS41 and EA-DOX-GNS41 were examined in DMEM containing 10% serum. Some atudies showed that peptides CP activity aften devreased in the presence of serum, because peptides may be trapped with proteins in serum. 200 μL of EF-DOX-GNS41, EA-DOX-GNS41 (25 nM peptide and 100 nM DOX conjugated GNS41) were added to HeLa and A549 $5x10^4$ cells in DMEM supplemented with 10% FBS and 1% PS and 3T3-L1 $5x10^4$ cells in DMEM supplemented with 10% DBS and 1% PS in each plate and incubated for 2 h. P-DOX-GNSs show the same CP activity in DMEM supplemented with 10% serum as that without serum (Figure 3-7). That is, EF-DOX-GNS41 showed high cell penetrability and EA-DOX-GNS41 showed low penetrability in HeLa cell. Both DOX-EF-GNS41 and DOX-EA-GNS41 show the high CP activity in A549 cell and the low CP activity in 3T3-L1 cell. From these data, it is confirmed that P-GNSs do not have effect of CP activity by serum.

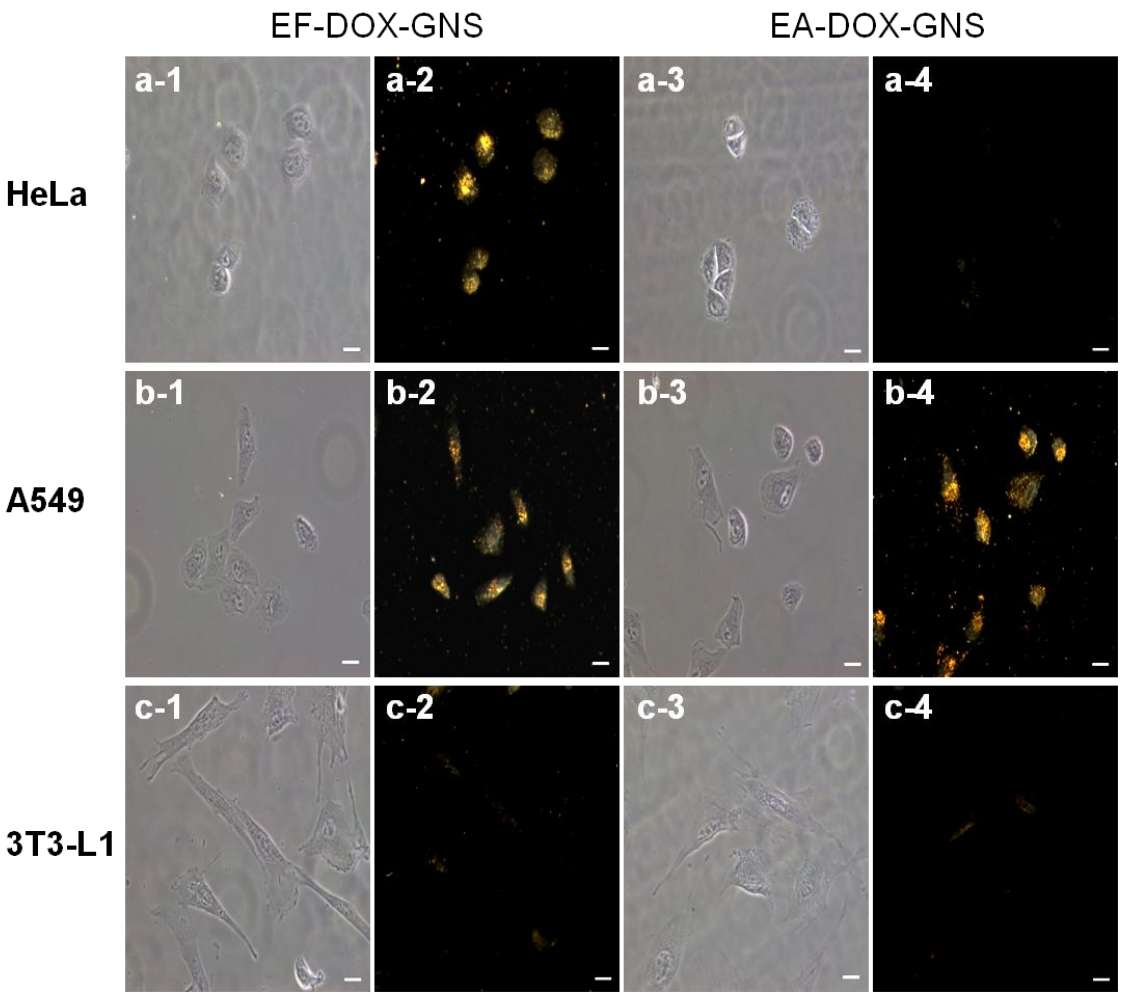

Figure 3-7 Bright field (1, 3) and dark field light scattering images (2, 4) of a) HeLa, b) A549, c) 3T3-L1 1 and 2 EF-DOX-GNS41, 3 and 4 EA-DOX-GNS41 in the presence of 10% serum.

3-4 Conclusions

In this chapter, nanoprobes composed of GNS41 and cell-penetrating α-helix peptides were constructed. The peptides were selected from an α-helix peptide library of 16-amino acids in the previous research [8-11] and showed varied CP activity with different amino acid sequences. These CPPs were conjugated to GNS41 via the thiol group of cysteine, thus enhancing the GNS cell penetrating activity by 25 nM. Peptides EF and EA have only one amino acid difference (Phe vs. Ala in the center of the sequence). The P-GNSs41 showed characteristic CP selectivity for three types of cells based on the CP activity of the peptides, which were elucidated by dark field imaging of the GNSs. Although the detail CP mechanism of the designed peptides is unclear, P-GNSs will be useful tools for clarification of the mechanism and interaction between them and cell surface, and for development of cell-specific CPPs.

In addition, selective cell death activity was induced using an anticancer drug, DOX, conjugated to the P-GNSs41. P-DOX-GNSs41 showed enhanced cell-selective cytotoxicity compared with free DOX in solution and DOX-GNS41 without peptides, which was attributed to the cell-selective internalization activity of peptides EF and EA. The P-GNSs41 could be applied to the construction of new cell-selective drug delivery systems in field of cancer research, which would be useful in cancer diagnosis and therapy development, with high efficiency and low toxicity.

References

[1] Sebbage V. Cell-penetrating peptides and their therapeutic applications. Bio-horizons 2009; 2: 64–72.

[2] Snyder EL, Dowdy SF. Cell penetrating peptides in drug delivery. Pharm Res-Dordr 2004; 21: 389–93.

[3] Pero SC, Shukla GS, Cookson MM, Flemer Jr S, Krag DN. Combination treatment with Grb7 peptide and doxorubicin or trastuzumab (herceptin) results in cooperative cell growth inhibition in breast cancer cells. Br J Cancer 2007; 96: 1520–5.

[4] Dilber MS, Phelan A, Aints A, Mohamed AJ, Elliott G, Edvard Smith CI, et al. Intercellular delivery of thymidine kinase prodrug activating enzyme by the herpes simplex virus protein, VP22. Gene Ther 1999; 6: 12–21.

[5] Hosotani R, Miyamoto Y, Fujimoto K, Doi R, Otaka A, Fujii, N, et al. Trojan p16 peptide suppresses pancreatic cancer growth and prolongs survival in mice. Clin Cancer Res 2012; 8: 1271–6.

[6] Xia H, Mao Q, Davidson B.L. The HIV tat protein transduction domain improves the biodistribution of β-glucuronidase expressed from recombinant viral vectors. Nat Biotechnol 2001; 19: 640-4.

[7] Bolhassani A. Potential efficacy of cell-penetrating peptides for nucleic acid and drug delivery in cancer. Biochimica et Biophysica Acta 2011; 1816: 232–46.

[8] Usui K, Tomizaki K, Mihara H. Protein-fingerprint data mining of a designed α-helical peptide array. Mol Biosyst 2006; 2: 417–20.

[9] Usui K, Kakiyama T, Tomizaki KY, Mie M, Kobatake E, Mihara H. Cell fingerprint patterns using designed α-helical peptides to screen for cell-specific toxicity. Bioorg Med Chem Lett 2011; 21: 6281–4.

[10] Usui K, Tomizaki K-Y, Mihara H. Screening of α-helical peptide ligands controlling a calcineurin-phosphatase activity. Bioorg Med Chem Lett 2007; 17: 167–71.

[11] Usui K, Kikuchi T, Mie M, Kobatake E, Mihara H. Systematic screening of the cellular penetration of designed alpha-helix peptides. Bioorg Med Chem 2013; 21: 2560–7.

[12] El-Sayed IH, Huang X, El-Sayed MA. Surface plasmon resonance scattering and absorption of anti-EGFR antibody conjugated gold nanoparticles in cancer diagnostics: applications in oral cancer. Nano Lett 2005; 5: 829–34.

[13] Kumar S, Harrison N, Richards-Kortum R, Sokolov K. Plasmonic nanosensors for imaging intracellular biomarkers in live cells. Nano Lett 2007; 7: 1338–43.

[14] Reinhard BM, Siu M, Agarwal H, Alivisatos AP, Liphardt J. Calibration of dynamic molecular rulers based on plasmon coupling between gold nanoparticles. Nano Lett 2005; 5: 2246–52.

[15] Aslan K, Lakowicz JR, Geddes CD. Plasmon light scattering in biology and medicine: new sensing approaches, visions and perspectives. Curr Opin Chem Biol 2005; 9: 538–44.

[16] You J, Zhang G, Li C. Exceptionally high payload of doxorubicin in hollow gold nanospheres for near-infrared light-triggered drug release. ACS Nano 2010; 4: 1033–41.

Chapter 4.

Cell-selective drug delivery system

using α-helix peptide-conjugated gold nanosperes

4-1 Introduction

In the chapter 3, EF and EA peptides were conjugated to a 41 nm GNS (P-GNS41), and evaluated their CP activities in three cell lines [1]. The P-GNS41 facilitated not only cell imaging at a low peptide concentration (25 nM: 1/100 of fluorophore-conjugated peptide [2]) with low cytotoxicity but also high cell selectivity according to the amino acid differences between the peptides. In addition, P-GNS41 exhibited drug delivery applicability via the conjugation of an anticancer drug, doxorubicin (DOX), to the GNS surface (P-DOX-GNS41), resulting in a 10-20% higher cell death activity than that of free DOX. To achieve greater cell death activity, a nanoprobe should accumulate around/in the cell nucleus and should have a high DOX release rate from the GNS surface. Therefore, recent studies have employed nuclear targeting using, for example, such as nuclear localization signal (NLS) peptides [3-7] and pH-sensitive materials [8-10]. Smaller-sized GNSs have also been reported to pass through the nuclear membrane [11-13].

In this chapter, the feasibility of using 25 nm GNS instead of 41-nm GNS [1] for nuclear targeting was examined. Five nanoprobes conjugated to either the TAT peptide or one of four peptides from the 16-amino acid peptide library (P-GNS25) were constructed. These five nanoprobes were coated with PEG (P-PEG-GNS25) to maintain the high stability during long incubations for nuclear targeting. P-PEG-GNSs are expected to be taken up by the cell via endocytosis, and the P-PEG-GNSs in endosomes or lysosomes may then migrate to the nucleus. Therefore, a pH-sensitive DOX-PEG is synthesized using a hydrazone linkage and conjugated to a 25 nm GNS (P-DOX-PEG-GNS25) to allow the controlled release of DOX from the vesicles under pH 5 (Figure 4-1) [14-16]. I demonstrated a more efficient cell-selective drug delivery system than that of P-GNS41 by examining the CP activities of five constructed P-PEG-GNS25 nanoprobes and the cell

death activities of P-DOX-PEG-GNS25 and then comparing the results with the activities of the TAT peptide.

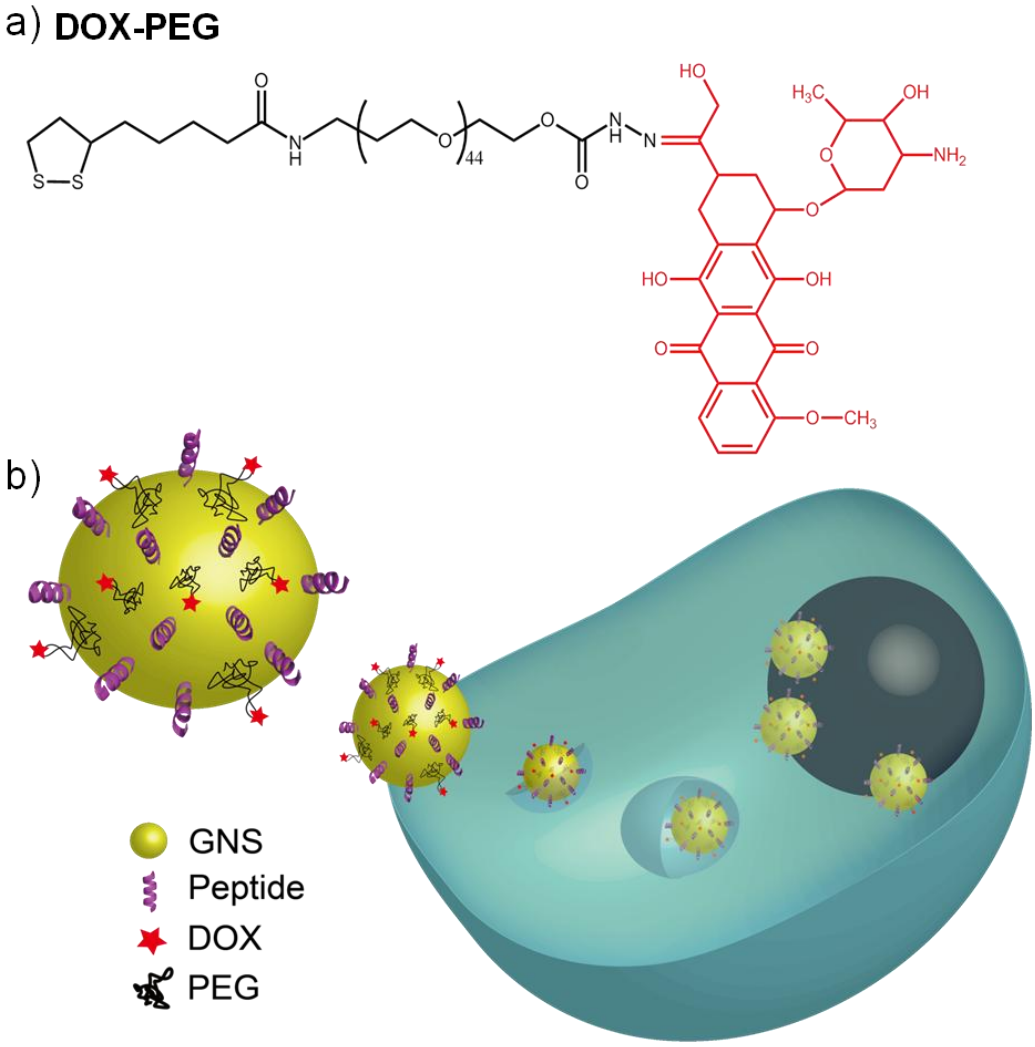

Figure 4-1 a) DOX-PEG having the pH-sensitive hydrazone linkage and the lipoic acid moiety for GNS conjugation and b) illustration of migration of peptides and DOX-PEG conjugated 25 nm GNS (P-DOX-PEG-GNS25) inside cell.

4-2 Materials and methods

4-2-1 Materials

Amino acids and reagents for peptide synthesis were purchased from Watanabe Chemical Industries, Kokusan Chemical and Hipep Laboratories. Gold (III) chloride trihydrate, penicillin-streptomycin (PS) and doxorubicin were obtained from Sigma-Aldrich. Trisodium citrate dihydrate was obtained from Koso Chemical. SH-PEG (Mw 2000) and HO-PEG-NH_2 (Mw 2000) were purchased from Nof Corporation. Dulbecco's modified eagle's medium (DMEM) was obtained from Wako Pure Chemicals Industries. OPTI-MEM was obtained from Gibco. Cell counting kit-8 (CCK-8) and DAPI were purchased from Dojindo Molecular Technologies. LysoTracker Green DND-26 was purchased from Invitrogen. SlowFade Gold Antifade Reagent was purchased from Life Technologies.

4-2-2 Gold nanosphere (GNS) synthesis

GNS was synthesized according to the Frens method [17]. After 50 mL of 0.03% gold (III) chloride trihydrate solution was started for boiling under reflux condition, added was 0.75 mL 3% trisodium citrate dehydrate solution as a reducing agents for 25 nm of GNS (1.5 nM). At this time, solution color was changed from yellow to colorless and then to red. The mixture was boiled for 20 min after color change and the heating was stopped. The diameter of the GNS was characterized by transmission electron microscopy (TEM, Hitachi H-7500 electron microscope) and UV-VIS spectroscopy. The absorption peak of 25 nm GNS was shown at 525 nm (Figure 4-2).

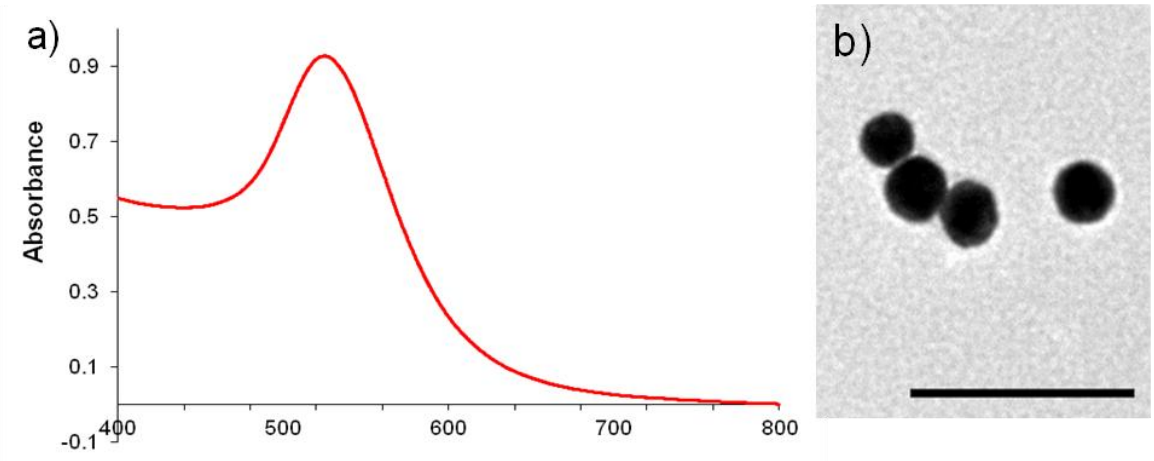

Figure 4-2 a) Surface plasmon absorption spectra and b) TEM image of 25 nm GNS

4-2-3 Synthesis of peptides (TAT, RF, RA, NLS)

Full sequence of peptides was shown in Figure 4-3. The peptides were synthesized by the conventional solid phase method using 9-fluorenylmethyloxycarbonyl (Fmoc) strategy [18]. The peptide chains were assembled on TGR resin using Fmoc amino acid derivatives (3 equiv), N,N-diisopropylethylamine (DIEA, 6 equiv), O-Benzotriazole-1-yl-N,N,N',N'-tetramethyl-uronium-hexafluoro phosphate (HBTU, 3 equiv), N-hydroxybenzotriazole mono hydrate (HOBt • H_2O, 3 equiv) in N-methylpyrrolidone (NMP) for coupling, and 20% piperidine (PPD)/NMP for Fmoc removal. To cleave the peptide from the resin and remove the side chain protecting groups, the resin of RF, RA, EF, EA peptides were treated with trifluoroacetic acid (TFA) / *m*-cresol / thioanisole / ethanedithiol (10 mL / 0.25 mL / 0.75 mL / 0.75 mL), and TAT and NLS pepetides were treated with TFA / H_2O / triisopropylsilane (10 mL / 0.2 mL / 0.2 mL). All peptides were purified by reverse-phase HPLC on a Cosmosil 5C18-ARII packed column (10 × 250 mm) by using a linear gradient of acetonitrile / 0.1% TFA at a flow rate of 3.0 mL/min. The peptides were identified satisfactorily by matrix-assisted laser desorption ionization time-of-flight mass spectrometry (MALDI TOF-MS) and electrospray ionization mass spectrometry (ESI-MS, Shimadzu LCMS-2010). Peptide RF, m/z obsd [M+H]+, 1937.9 m/z calcd [M+H]+ 1937.5; Peptide RA, m/z obsd [M+H]+ 1862.4, m/z calcd [M+H]+ 1861.1; Peptide TAT, m/z obsd [M+H]+ 1555.9, m/z calcd [M+H]+ 1556.9, Peptide NLS, m/z obsd [M+H]+ 1270.6, m/z calcd [M+H]+ 1271.6.

Name	Sequences	GNS conjugate
RF	GLKKLA**R**L**F**HKLLKLGC-NH_2	RF-PEG-GNS25
RA	GLKKLA**R**L**A**HKLLKLGC-NH_2	RA-PEG-GNS25
EF	GLKKLA**E**L**F**HKLLKLGC-NH_2	EF-PEG-GNS25
EA	GLKKLA**E**L**A**HKLLKLGC-NH_2	EA-PEG-GNS25
TAT	GRKKRRQRRRGC-NH_2	TAT-PEG-GNS25
NLS	CGGGPKKKRKVGG-NH_2	NLS-PEG-GNS25

Figure 4-3 Sequences of RF, RA, EF, EA, and TAT peptides and peptides conjugated with GNS.

4-2-4 Construction of PEG-GNS25, P-PEG-GNS25, and P-DOX-PEG-GNS25 nanoprobes

PEG-GNS25 was constructed by adding 3 μM SH-PEG (Mw 2000) to 25 nm GNS (1.5 nM), and P-PEG-GNS25 was constructed using each 25 nM peptides (TAT, RF, RA, EF, EA, and NLS), and 3 μM SH-PEG to 25 nm GNS (1.5 nM) by shaking for 2 h at room temperature. P-DOX-PEG-GNS25 were synthesized using each 25 nM peptides (TAT, RF, RA, EF, and EA), and 3 μM DOX-PEG (described in chapter 4-2-8) to 25 nm GNS (1.5 nM) by shaking for 2 h at room temperature. After 2 h, each of the samples was washed by centrifuge at 12,000 rpm for 15 min with OPTI-MEM.

4-2-5 Cytotoxicity of peptide-conjugated GNS25 (P-PEG-GNS25)

HeLa cells $5x10^3$ in 100 μL of Dulbecco's modified eagle medium (DMEM) supplemented with 10% fetal bovine serum (FBS) and 1% penicillin-streptomycin (PS) were incubated in 96 well plate for 24 h at 37℃ under 5% CO_2. After washing 3 times with OPTI-MEM, 100 μL P-PEG-GNS samples (PEG-GNS, TAT-PEG-GNS, RF-PEG-GNS, RA-PEG-GNS, EF-PEG-GNS and EA-PEG-GNS) were added. They were incubated for 24 h at 37℃ under 5% CO_2. After washing 3 times with OPTI-MEM, 10 μL of cell counting kit 8 (CCK-8) was added, and the mixture was incubated for 1 h at 37℃ under 5% CO_2. The absorption intensity was detected using a plate reader (ARVO MX 1420 multilabel counter, Perkin Elmer) at 450 nm, and the cell viability was calculated as 100 % cells viability of OPTI-MEM.

4-2-6 Cell penetrating (CP) activity of PEG-GNS and P-PEG-GNS

HeLa cells and A549 cells were cultured in DMEM supplemented with 10% FBS and 1% PS, and 3T3-L1 cells was cultured in DMEM supplemented with 10% Donor Bovine Serum (DBS) and 1% PS to prevent the cell differentiation at 37℃ under 5% CO_2. For cell labeling, $2x10^4$ cells were placed on 22x22 mm cover slip in 6 well cell culture plates and cultured overnight at 37℃ under 5% CO_2. After washing twice with OPTI-MEM, 200 μL of PEG-GNS, TAT-PEG-GNS, RF-PEG-GNS, RA-PEG-GNS, EF-PEG-GNS, EA-PEG-GNS, and NLS-PEG-GNS were added in each plate and incubated for 24 h. They were washed twice with OPTI-MEM, coated with 90% glycerol and sealed to slide glass. Dark-field images based on elastic light scattering were taken using a Nikon microscope (Ti-U) with an immersion dark field condenser.

4-2-7 Localization analysis of P-PEG-GNS25 in cell using lysotracker

$2x10^4$ HeLa cells were placed on 22x22 mm cover slip in 6 well cell culture plates and cultured overnight at 37℃ under 5% CO_2. After washing twice with OPTI-MEM, 200 μL of EF-PEG-GNS was added and incubated for 24 h. Cells were washed twice with OPTI-MEM, added the 5 μM LysoTracker Green DND-26 was added and incubated for 4 h. After washing twice with OPTI-MEM, they were incubated with 4% paraformaldehyde for 15 min to fix the cells. After washing twice with OPTI-MEM, cells were incubated with 250 nM DAPI for 5 min for staining cell nucleus. They were washed twice with OPTI-MEM, coated with Slowfade gold antifade reagent and sealed to slide glass. Dark field images based on elastic light scattering and fluorescent images were taken using a Nikon microscope (Ti-U) with an immersion dark field condenser.

4-2-8 pH-responsive DOX-PEG synthesis

PEG-DOX was synthesized according to the previous papers [10-12]. α-Lipoic acid (136 mg, 0.66 mmol), N,N'-dicyclohexylcaboiimide (136 mg, 0.66 mmol), hydroxysuccinimide (59.5 mg, 0.52 mmol) and triethylamine (162 μL, 1.16 mmol) were added to HO-PEG-NH_2 (1.0 g, 0.50 mmol, Mw 2000) in anhydrous CH_2Cl_2 (5 mL). The mixture was stirred at RT for 2 days, and then filtrated to remove dicyclohexylurea. The bottom solution was precipitated with ethylether, and then dried under vacuum overnight to produce α-lipoyl **ω**-hydroxyl poly(ethylene glycol) (LA-PEG-OH) with a yield of 92%.

LA-PEG-OH (0.80 g, 0.37 mmol) and triethylamine (118 μl, 0.85 mmol) in 20 mL CH_2Cl_2 were stirred at 0℃. To this solution was added dropwise *p*-nitrophenyl chloroformate (226 mg, 1.12 mmol) in 10 mL CH_2Cl_2. The reaction was performed at 0℃ for 1 h and 48 h at room temperature under N_2 atmosphere. This solution was diluted by CH_2Cl_2 and washed with brine solution for three times. The organic phase was dried with sodium sulfate and evaporated, precipitated into diethylether and dried under vacuum for 1 h to produce LA-PEG-NPC with a yield of 69%.

LA-PEG-NPC (600 mg, 0.25 mmol) in 20 mL CH_2Cl_2 was added dropwise hydrazine monohydrate (127 μL, 2.53 mmol). The reaction was performed for 48 h at room temperature and washed with brine solution. The organic phase was dried with sodium sulfate, evaporated and dried under vacuum overnight to give LA-PEG-Hyd with a yield of 83%.

LA-PEG-Hyd (38 mg, 0.02 mmol) and doxorubicin (10 mg, 0.02 mmol) in 15 mL anhydrous MeOH was reacted in the presence of a drop of trifluoroacetic acid at 60℃ overnight. The product was obtained by gel filtration (Sephadex LH-20) and lyophilization with a yield of 89% of LA-PEG-DOX (α-lipoyl-ω-doxorubicinyl poly(ethylene glycol)

with a hydrazone linkage), LA-PEG-DOX was named by DOX-PEG in the later section. Because DOX-PEG is pH-response, DOX was released in acidic condition from PEG via the hydrazone linkage. The reaction of each step was checked using NMR spectroscopy. The DOX content in DOX-PEG was approximately 3.3% of the PEG unit.

4-2-9 DOX release test of DOX-PEG-GNS25 at pH 4.5 and 7.4

10 μM DOX-PEG was added to 25 nm GNS (1.5 nM) and the solution was shaken for 2 h at room temperature. DOX-PEG-GNS25 was incubated in acetate buffer (pH 4.5) and PBS (pH 7.4). These solutions were detected by the fluorescent emission intensity at 560 nm with 465 nm excitation to check the released DOX amount using fluorescent intensity of DOX according to the incubation time.

4-2-10 Cell death activity of P-DOX-PEG-GNS25

HeLa and A549 $2x10^3$ cells in 100 μL of DMEM supplemented with 10% FBS and 1% PS and 3T3-L1 $2x10^3$ cells in 100 μL of DMEM supplemented 10% DBS and 1% PS were incubated in 96 well plate for 24 h at 37℃ under 5% CO_2. After washing 3 times with OPTI-MEM, added were 100 μL of the PEG-GNS25, TAT-, RF-, RA-, EF- and EA-DOX-PEG-GNS25 (25 nM peptide and DOX-PEG: DOX content: 10, 50, and 100 nM to GNS25). They were incubated for 24 h at 37℃ under 5% CO_2. Cell plate was incubated for 24 h at 37℃ under 5% CO_2 for release of DOX after washing 3 times with OPTI-MEM. After 10 μL of CCK-8 was added, the mixture was incubated for 1 h at 37℃ under 5% CO_2. The absorption intensity was detected using the plate reader at 450 nm.

4-3 Results and discussion

4-3-1 Peptide and PEG conjugated GNS (P-PEG-GNS25) for nuclear targeting

Four types of α-helical peptides—RF, RA, EF, and EA—were selected from α-helical peptide library of Mihara group [1,2,19-21]. Although contained different Phe/Ala and Arg/Glu residues at two defined positions in the 16-amino amino acid sequences, these peptides exhibited different CP activities in three cell lines in the previous research [2]. Figure 4-3 shows the five peptide sequences, which include the four types of α-helical peptide (RF, RA, EF, and EA peptides) and the TAT peptide. These peptides synthesized by adding a Cys residue to the C-terminus and were then conjugated to a 25 nm GNS by linking the -SH of the Cys to gold surface. This linkage was chosen because the N-terminus conjugated peptide-GNS41 exhibited a different CP activity in the chapter 3 [1]. A 25 nm GNS was selected instead of a 41 nm GNS to study in this chapter because these particles might have different CP activities because of their size difference. This possibility using 16 nm, 25 nm, and 41 nm GNSs conjugated to the EF peptide was evaluated. First, the EF peptide-conjugated 41 nm GNS was taken up by HeLa cells and localized throughout the entire cell, as discussed in a later section and shown in Figure 4-7. The EF peptide-conjugated 16 nm GNS localized around the nucleus of the HeLa cells, but this nanoparticle also exhibited high CP activity without the peptide. The 16 nm GNS without the peptide penetrated the nuclear membrane and accumulated around and inside the nucleus (Figure 4-4 a1-4). The EF peptide-conjugated 25 nm GNS accumulated around the nucleus after 24 h without the addition of another peptide, such as an NLS peptide (Figure 4-4 b3 and 4 and Figure 4-7c and d). Because DOX acts on DNA in the cell nucleus, it can be hypothesized that the nucleus targeting ability of P-GNS25 would induce high cell

death by releasing the DOX around the nucleus. Therefore, I chose a GNS size of 25 nm, instead of the 41 nm GNS used in the chapter 3, and conjugated it to a PEG chain to maintain its stability during interactions with cells [22,23]. Then, 25 nM peptides (TAT, RF, RA, EF, or EA) and 3 μM PEG were conjugated to GNS25 to create P-PEG-GNS25, which was stable for several months at room temperature in OPTI-MEM medium.

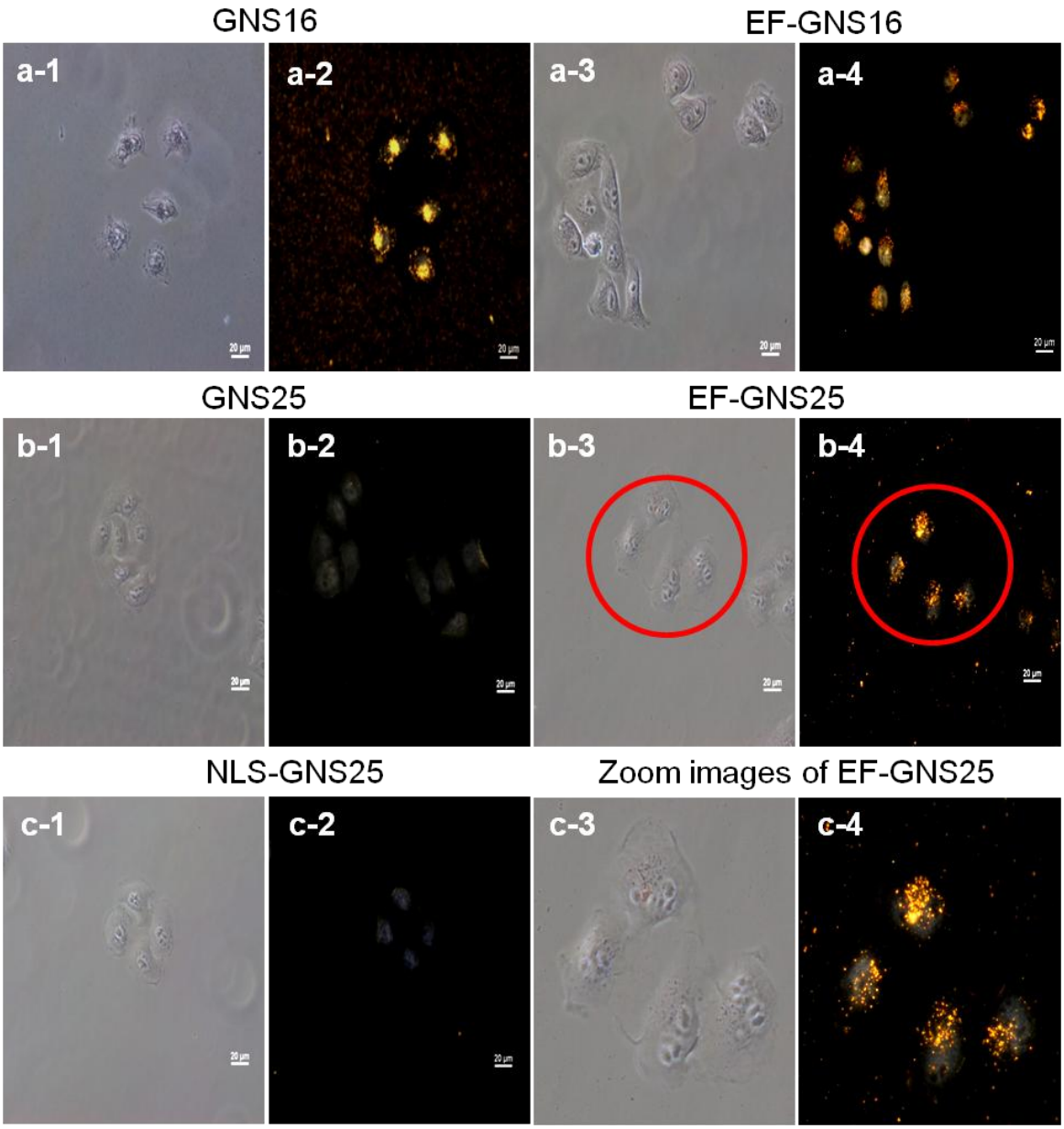

Figure 4-4. Bright field (1 and 3) and dark field light scattering images (2, 4) of in HeLa. a-1 and a-2: GNS16, a-3 and a-4: EF-GNS16, b-1 and b-2: GNS25, and b-3 and b-4: EF-GNS25, c-1 and c-2: NLS-GNS25, and c-3 and a-4: zoom images of red circles of b-3and b-4.

4-3-2 Cytotoxicity against HeLa cells and dark field images in HeLa, A549, and 3T3-L1 cells after incubation with P-PEG-GNS25

P-PEG-GNS25 showed more than 95% cell viability, and the viability of cells in OPTI-MEM alone was 100% (Figure 4-5). These results demonstrated the high cell compatibility of P-PEG-GNSs.

Figure 4-6 shows the bright field and light scattering images of HeLa, A549, and 3T3-L1 cells after 24 h incubation with PEG-GNS25 and P-PEG-GNS25. PEG-GNS25 without peptide showed low CP activity in HeLa (Figure 4-6 a-1 and a-2), A549 (b-1 and b-2), and 3T3-L1 cells (c-1 and c-2). In contrast, TAT-PEG-GNS25 showed high CP activity in HeLa (Figure 4-6 a-3 and a-4), A549 (b-3 and b-4), and 3T3-L1 cells (c-3 and c-4). RF-PEG-GNS25 and EF-PEG-GNS25 showed high CP activity in HeLa and A549 cells (Figure 4-6 a-5 and a-6 [RF-PEG-GNS25], a-9 and a-10 [EF-PEG-GNS25], b-5 and b-6 [RF-PEG-GNS25], and b-9 and b-10 [EF-PEG-GNS25]) and low CP activity in 3T3-L1 cells (c-5 and c-6 [RF-PEG-GNS25] and c-9 and c-10 [EF-PEG-GNS25]). EA-PEG-GNS25 showed high CP activity in A549 cells (Figure 4-6 b-11 and b-12) and low CP activity in HeLa (a-11 and a-12) and 3T3-L1 cells (c-11 and b-12). The CP activities and cell selectivities of RF-, EF-, and EA-PEG-GNS25 were similar to those of the free peptides in the previous study [2]; however, the CP activity of RA-PEG-GNS25 tended to differ from that of the free RA peptide. RA-PEG-GNS25 showed high CP activity in HeLa cells only (Figure 4-6 a-7 and a-8) and low CP activity in A549 (b-7 and b-8) and 3T3-L1 cells (c-7 and c-8). However, the free RA peptides showed high CP activity in all three cell lines, HeLa (scored: +++), A549 (scored: ++), and 3T3-L1 (scored: +++) [2]. The different CP activity exhibited by RA-PEG-GNS25 may be due to the directivity of the RA peptide conjugated to GNS compared with the free RA peptide on the cell surface or to the

different peptide densities of RA-PEG-GNS25 (25 nM) and the free RA peptide (2 μM). Figure 4-6 demonstrates that RF-, RA-, EF-, and EA-PEG-GNS25 showed not only high CP activities similar to that of TAT-PEG-GNS25 but also cell selectivity according to peptide sequences with one or two amino acid differences.

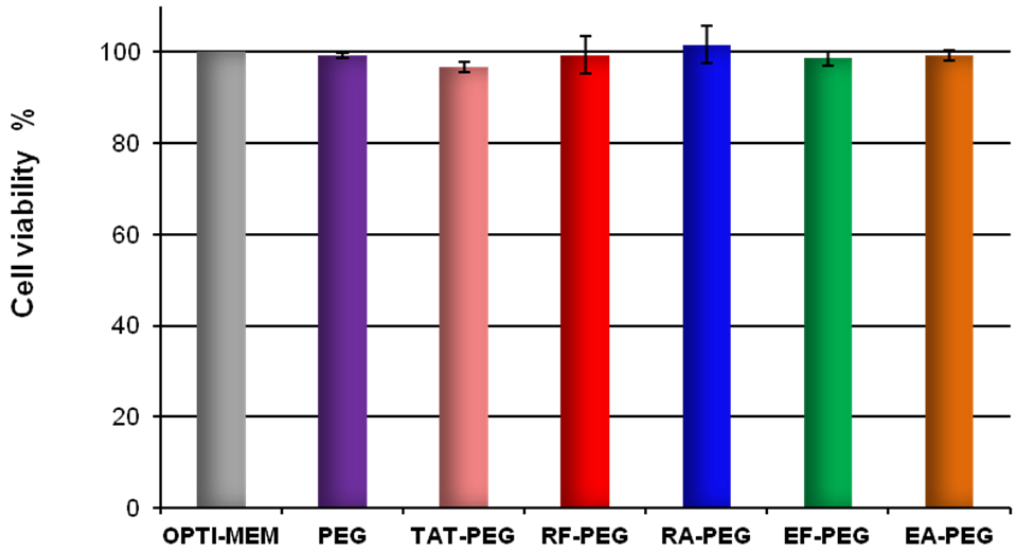

Figure 4-5. In vitro cytotoxicity test of PEG: 3 μM PEG conjugated GNS25, TAT-PEG: 25 nM TAT peptide-, RF-PEG: 25 nM RF peptide-, RA-PEG: 25 nM RA peptide-, EF-PEG: 25 nM EF peptide-, and EA-PEG: 25 nM EA peptide and 3 μM PEG conjugated GNS25 against HeLa cell.

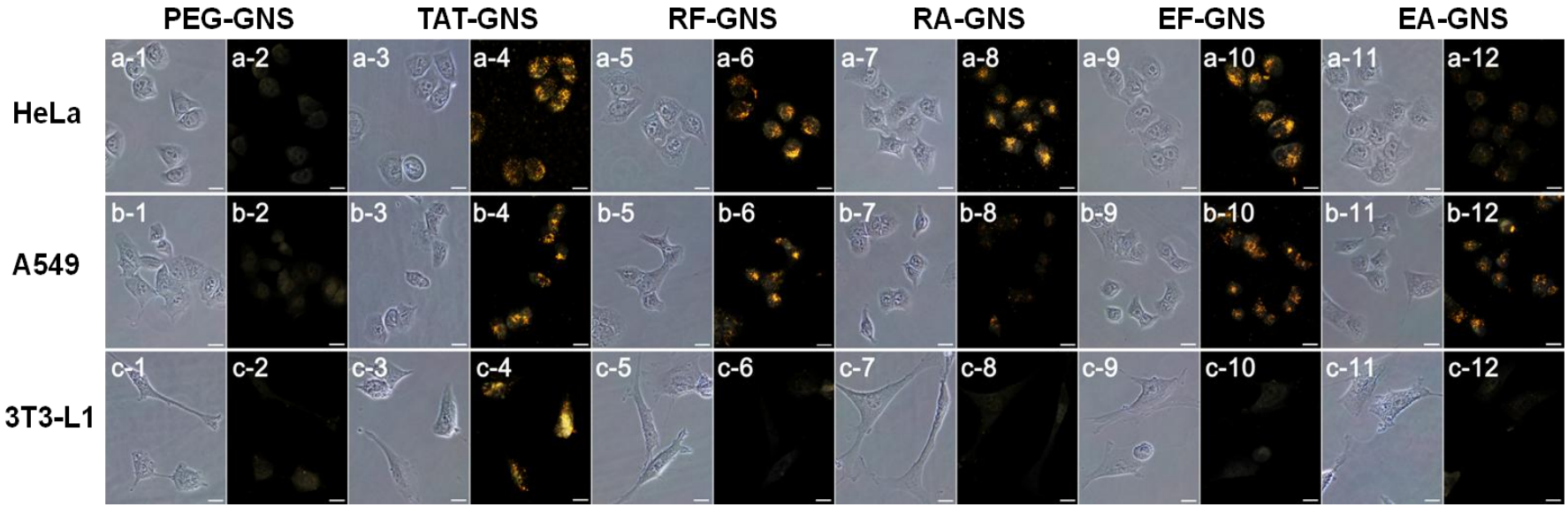

Figure 4-6. Bright field (1, 3, 5, 7, 9, 11) and dark field light scattering images (2, 4, 6, 8, 10, 12) of a: HeLa, b: A549, c: 3T3-L1 cells. 1 and 2: PEG-GNS25, 3 and 4: TAT-PEG-GNS25, 5 and 6: RF-PEG-GNS25, 7 and 8: RA-PEG-GNS25, 9 and 10: EF-PEG-GNS25, and 11 and 12: EA-PEG-GNS25.

4-3-3 Cellular localization of P-PEG-GNS25 compare with P-GNS41

EF-PEG-GNS25 accumulated around the cell nucleus in HeLa (Figure 4-7c) and A549 cells (Figure 4-7d). In contrast, EF-GNS41 localized throughout the entire cells in HeLa (Figure 4-7a) and A549 cells (Figure 4-7b). To investigate the P-PEG-GNS25 uptake process, HeLa cells were stained with LysoTracker Green after incubation with EF-PEG-GNS25. Figure 4-8 shows the following cell images: a) bright field, b) dark field, c) LysoTracker Green fluorescence, and d) a merged image (DAPI staining of the nucleus). The dark field image of GNS25 (Figure 4-8b) and the fluorescent LysoTracker image (Figure 4-8c) overlapped in similar regions around the nucleus. P-PEG-GNS25 was definitively demonstrated to be trapped inside endosomes or lysosomes after its uptake by the endocytotic mechanism and to subsequently accumulate around the nucleus.

Figure 4-9 showed the HeLa cells images after 24 h incubation with a) EF-PEG-GNS25 and b) 2μM EF peptide and EF-PEG-GNS25. 2μM EF peptide was incubated with EF-PEG-GNS25 to know whether or not the free peptide competes with the cell internalization of EF-PEG-GNS25. As a result, uptake of EF-PEG-GNS25 was not inhibited by the free EF peptide. EF-PEG-GNS25 showed the similar CP activity whether EF peptide exists or not (Figure 4-9). It demonstrated that EF-PEG-GNS25 has much stronger interaction ability with cell than the free peptide, because it was conjugated with multi-peptides on GNS. Another possibility is that the P-GNS has different mechanisms for penetration from the free peptide.

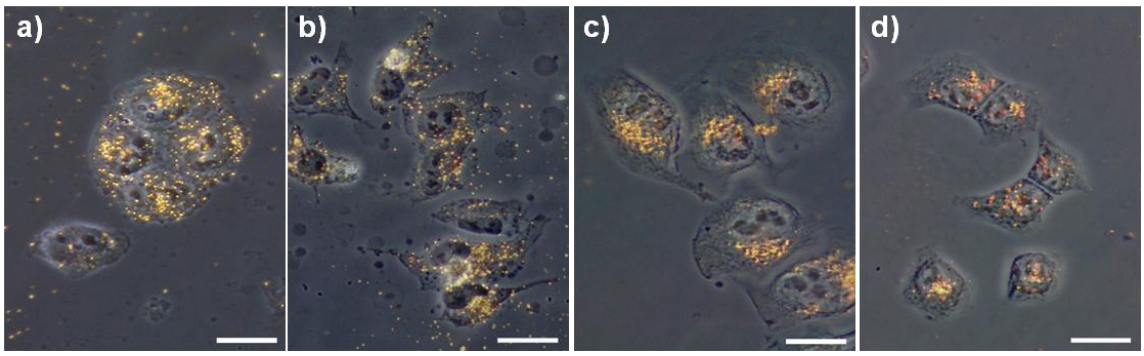

Figure 4-7. Merge images of bright field and dark field light scattering images of a: EF-GNS41 in HeLa, b: EF-GNS41 in A549, c: EF-PEG-GNS25 in HeLa cell and d: EF-PEG-GNS25 in A549 cell.

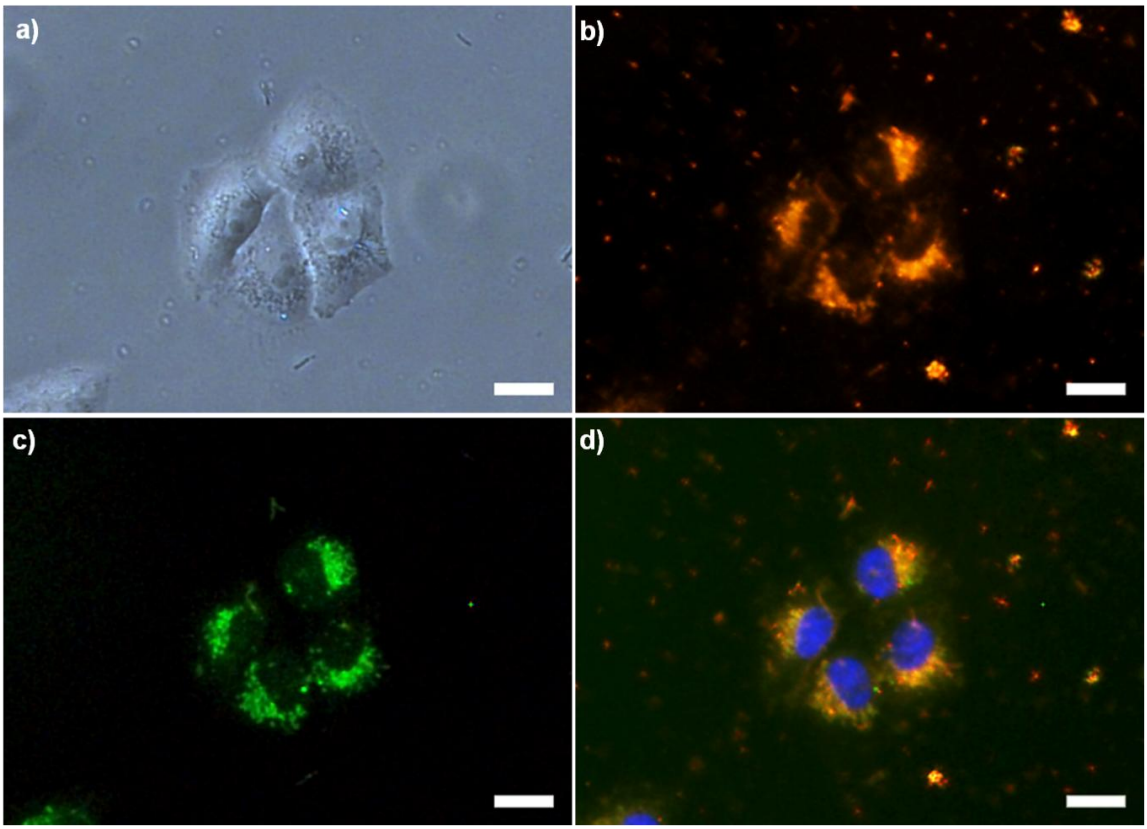

Figure 4-8. Fluorescence and dark field microscope images of HeLa cells after incubation of P-PEG-GNS25, LysoTracker green, and DAPI. a) bright field image, b) dark field image, c) fluorescent image of Lysotracker, and d) merge image (cell nucleus was stained with DAPI).

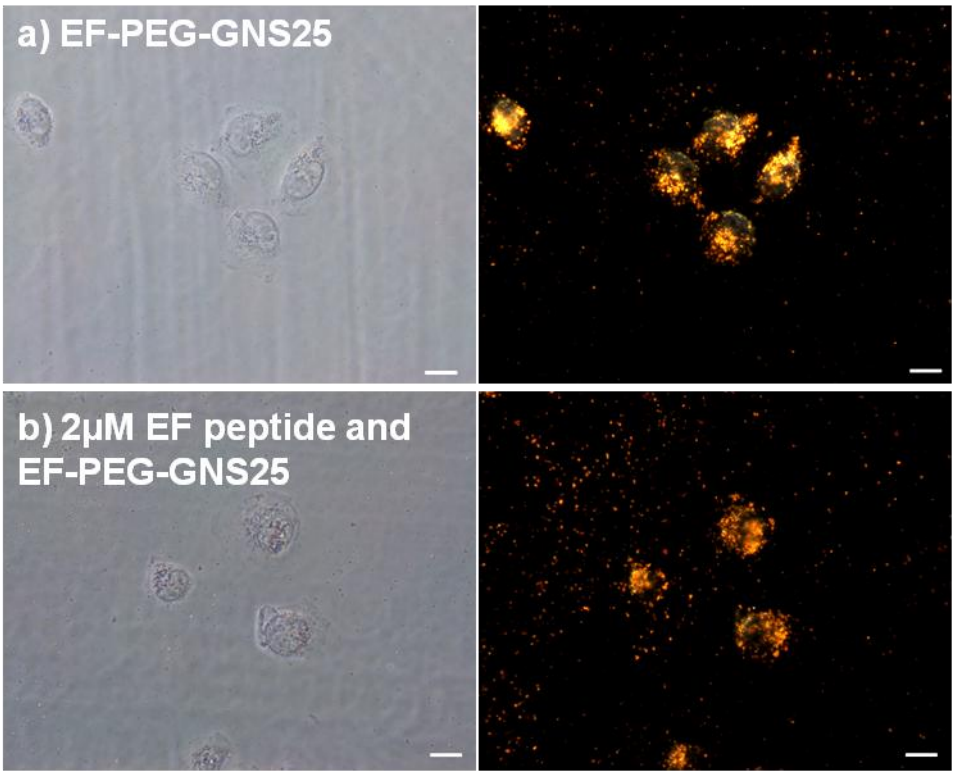

Figure 4-9. Bright field (left panel) and dark field (right panel) images of HeLa cells after incubation with a) EF-PEG-GNS25 and b) 2μM EF peptide and EF-PEG-GNS25.

4-3-4 DOX release from GNS after incubation at pH 4.5 and 7.4

The pH-responsive DOX-PEG-GNS25 was prepared, and the release of DOX from the GNS surface was examined by observing the fluorescence intensity of DOX according to changes in pH. Figure 4-10 shows the changes in DOX fluorescence intensity according to incubation time at pH 4.5 and 7.4. Figure 4-10a shows a significant fluorescence intensity increase at pH 4.5 within 2 h. After 24 h at pH 4.5, the 80% of the DOX was confirmed to have been released from DOX-PEG-GNS25 (Figure 4-10b). However, DOX-PEG-GNS25 did not show significant changes in fluorescence intensity at pH 7.4 after 48 h (Figure 4-10b). These data confirm that the DOX can be released from the synthesized DOX-PEG-GNS25 according to the pH change from neutral to acidic conditions.

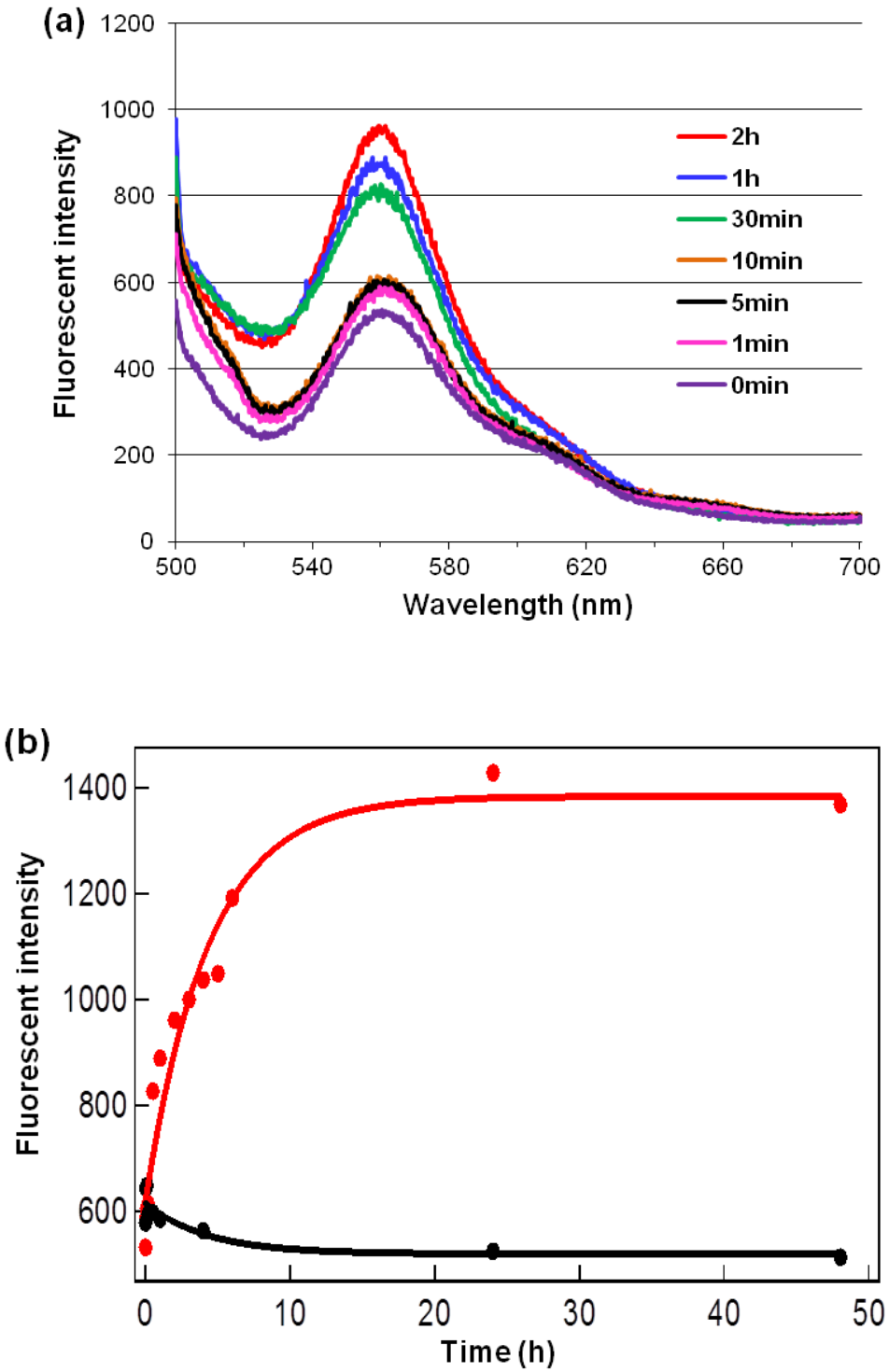

Figure 4-10. a) Fluorescence emission spectra of DOX-PEG-GNS25 incubated in acetate buffer (pH 4.5). b) DOX release analysis at pH 4.5 (red line) and pH 7.4 (black line) according to the incubation time.

4-3-5 Selective cell death activity of P-DOX-PEG-GNS

P-PEG-GNS25 showed cell-selective penetrating activity in the HeLa, A549, and 3T3-L1 cell lines. Five peptides (TAT, RF, RA, EF, and EA) and synthesized DOX-PEG were conjugated to 25 nm GNS to construct five nanoprobes: TAT-, RF-, RA-, EF-, and EA-DOX-PEG-GNS25 (P-DOX-PEG-GNS25), respectively. Using these five nanoprobes, cell-selective death activity was demonstrated by DOX release in the three cell lines. Figure 4-11 shows the cell death activity of the peptide-conjugated DOX-PEG-GNS25, TAT-PEG-DOX-GNS25 (pink bar), RF-DOX-PEG-GNS25 (orange bar), RA-DOX-PEG-GNS25 (light blue bar), EF-DOX-PEG-GNS25 (red bar) and EA-DOX-PEG-GNS25 (blue bar) with different DOX concentrations (10, 50, and 100 nM) in the HeLa, A549, and 3T3-L1 cell lines. The green bar shows the cell death activity of the free DOX solution. In the HeLa cells, the peptides with high CP activity showed higher cell death induction than the free DOX solution (80% cell viability at 100 nM). The cell viability of TAT-DOX-PEG-GNS25 was 44%; RF-DOX-PEG-GNS25, 46%; RA-DOX-PEG-GNS, 46%; and EF-DOX-PEG-GNS25, 40%. The HeLa cells showed the same tendency at 50 nM (cell viability of DOX solution: 88%, TAT-DOX-PEG-GNS25: 60%, RF-DOX-PEG-GNS25: 58%, RA-DOX-PEG-GNS25: 57%, and EF-DOX-PEG-GNS25: 59%) and at 10 nM (DOX solution: 99%, TAT-DOX-PEG-GNS25: 74%, RF-DOX-PEG-GNS25: 70%, RA-DOX-PEG-GNS25: 71%, EF-DOX-PEG-GNS25: 77%). TAT-, RF-, RA-, and EF-DOX-PEG-GNS25 showed approximately 20%-40% higher cell death activity than the free DOX solution under the same conditions, whereas EA-DOX-PEG-GNS25 showed low cell death activity in HeLa cells: 74% (100 nM), 81% (50 nM), and 89% (10 nM) (Figure 4-11a). In A549 cells (Figure 4-11b), TAT-, RF-, EF-, and EA-DOX-PEG-GNS25, all with high CP activity, showed cell death activities approximately 20-40% higher than those of

the free DOX solution under the same conditions. RA-DOX-PEG-GNS25 had lower cell death activity than the other P-DOX-PEG-GNSs25 at all concentrations in the A549 cells. In 3T3-L1 cells (Figure 4-11c), all the α-helical peptides, RF-, RA-, EF-, and EA-DOX-PEG-GNS25, showed low cell death activities, with more than 90% cell viability. TAT-PEG-GNS25 showed high CP activity in 3T3-L1 cells, but its cell death activity in 3T3-L1 cells was not higher than in HeLa or A549 cells. DOX showed different cell death activity levels by cell type [24]. The TAT peptide did not show the cell selectivity. The results of the cell death activity assays for P-DOX-PEG-GNSs25 corresponded with the CP activity results of TAT-, RF-, RA-, EF-, and EA-PEG-GNS25, and P-DOX-PEG-GNSs25 showed higher cell death induction than P-GNS41 [1]. It was thought that P-DOX-PEG-GNSs25 could efficiently release DOX using the pH-responsive PEG on GNS25, thereby effectively inducing cell death due to its accumulation around the cell nucleus compared with P-GNS41. The α-helical peptides-GNS25 conjugates, RF-, RA-, EF-, and EA-DOX-PEG-GNS25, indicated not only showed similar CP and cell death activities compared with the typical CPP, the TAT peptide, but also showed cell selectivity by cell type and peptide sequence. I demonstrated that P-DOX-PEG-GNSs25 has the potential to lead to the development of a novel cell-selective drug delivery system.

a) HeLa cell

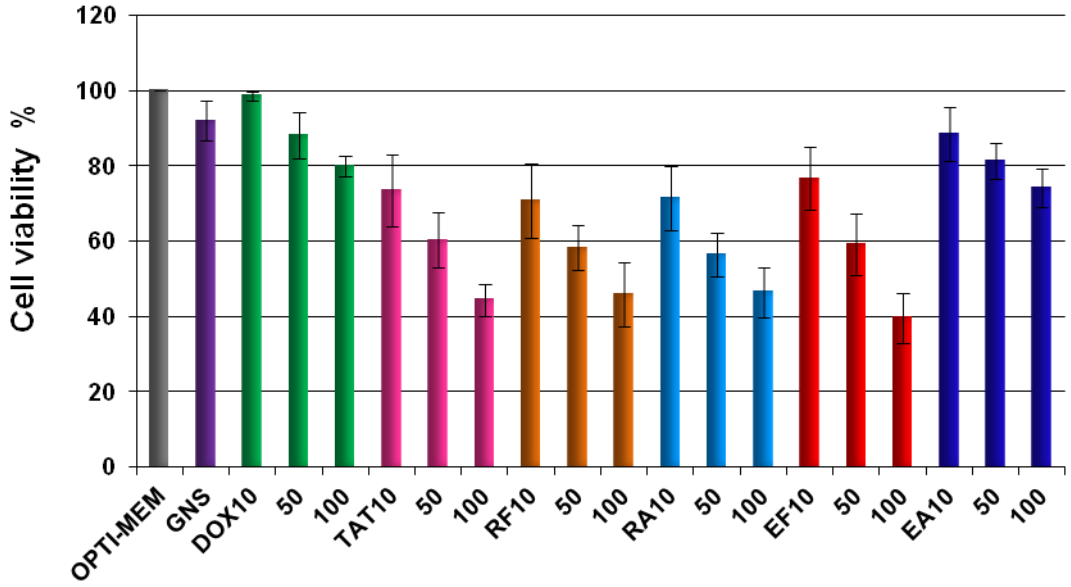

b) A549 cell

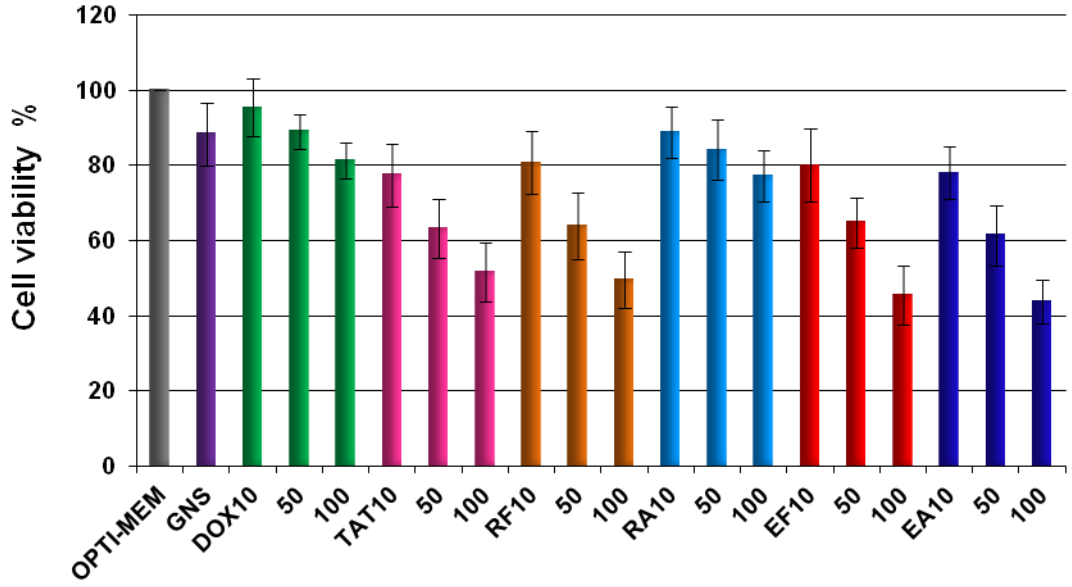

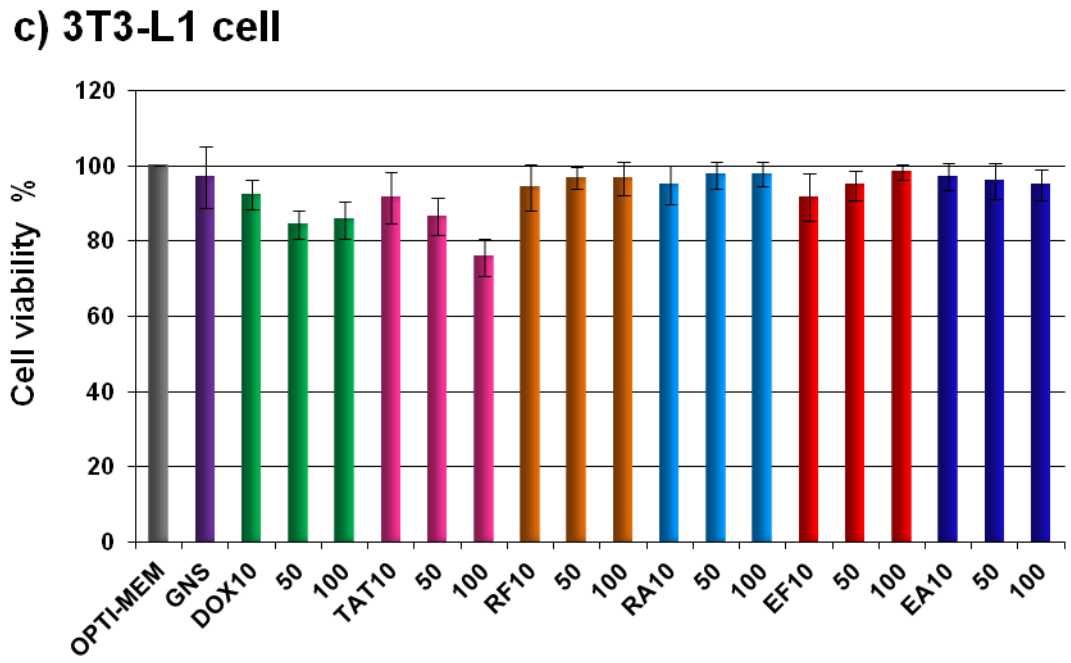

Figure 4-11. Cell death activity on (a) HeLa, (b) A549, (c) 3T3-L1 of free DOX solution, TAT-, RF-, RA-, EF-, EA- DOX-PEG-GNS25 on the 3 kinds of DOX concentration of 10, 50, 100 nM. Grey bar: OPTI-MEM, violet bar: PEG-GNS25, green bar: free DOX solution, pink bar: TAT-DOX-PEG-GNS25, orange bar: RF-DOX-PEG-GNS25, light blue bar: RA-DOX-PEG-GNS25, red bar: EF-DOX-PEG-GNS25, and blue bar: EA-DOX-PEG-GNS25.

4-4 Conclusions

In this chapter, five nanoprobes by conjugating either the TAT peptide or one of four α-helical peptides, RF, RA, EF, and EA, to a 25 nm GNS were constructed. The four α-helical peptide-conjugated nanoprobes showed similar CP and cell death activities compared with the TAT peptide in three cell lines, HeLa, A549, and 3T3-L1, with high cell selectivity according to cell type and peptide sequence. Moreover, P-DOX-PEG-GNS25, which contained a pH-sensitive DOX linkage, showed levels of cell death induction by DOX (20%-40%) that were approximately two times higher than those (10%-20%) described in the chapter 3 in which the EF and EA peptides were conjugated to 41 nm GNS [1]. The 25 nm GNS complexes accumulated around the cell nucleus, where DOX was effectively released from the GNS, resulting in a higher induction of cell death. These data indicate that P-PEG-GNSs25 could be applied to the construction of novel, highly efficient, less toxic cell-selective drug delivery systems for cancer research, including cancer diagnosis and therapy development.

Reference

[1] Park H, Tsutsumi H, Mihara H. Cell penetration and cell-selective drug delivery using α-helix peptides conjugated with gold nanoparticles. Biomaterials 2013; 34: 4872–9.

[2] Usui K, Kikuchi T, Mie M, Kobatake E, Mihara H. Systematic screening of the cellular penetration of designed alpha-helix peptides. Bioorg Med Chem 2013; 21: 2560-7.

[3] Tkachenko AG, Xie H, Coleman D, Glomm W, Ryan J, Anderson MF, et al. Multifunctional gold nanoparticle-peptide complexes for nuclear targeting. J Am Chem Soc 2003; 125: 4700–1.

[4] Kang B, Mackey MA, El-Sayed MA. Nuclear targeting of gold nanoparticles in cancer cells induces DNA damage, causing cytokinesis arrest and apoptosis. J Am Chem Soc 2010; 132: 1517–9.

[5] Xie W, Wang L, Zhang Y, Su L, Shen A, Tan J, et al. Nuclear targeted nanoprobe for single living cell detection by surface-enhanced Raman scattering. Bioconjug Chem 2009; 20: 768–73.

[6] Oyelere AK, Chen PC, Huang X, El-Sayed IH, El-Sayed MA. Peptide-conjugated gold nanorods for nuclear targeting. Bioconjug Chem 2007; 18: 1490–7.

[7] Qian W, Huang X, Kang B, El-Sayed M a. Dark-field light scattering imaging of living cancer cell component from birth through division using bioconjugated gold nanoprobes. J Biomed Opt 2011; 15: 046025.

[8] Gao W, Chan JM, Farokhzad OC. pH-Responsive nanoparticles for drug delivery. Mol Pharmaceutics 2010; 7: 1913–20.

[9] Jiang T, Zhang Z, Zhang Y, Lv H, Zhou J, Li C, et al. Dual-functional liposomes based on pH-responsive cell-penetrating peptide and hyaluronic acid for tumor-targeted anticancer drug delivery. Biomaterials 2012; 33: 9246–58.

[10] Urano Y, Asanuma D, Hama Y, Koyama Y, Barrett T, Kamiya M, et al. Selective molecular imaging of viable cancer cells with pH-activatable fluorescence probes. Nat Med 2009; 15: 104–9.

[11] Oh E, Delehanty JB., Sapsford KE, Susumu K, Goswami R, Blanco-Canosa JB., et al. Cellular uptake and fate of PEGylated gold nanoparticles is dependent on both cell-penetration peptides and particle size. ACS Nano 2011; 5: 6434–48.

[12] Thurn KT, Brown EMB, Wu A, Vogt S, Lai B, Maser J, et al. Nanoparticles for applications in cellular imaging. Nanoscale Res Lett 2007; 2: 430–41.

[13] Huang K, Ma H, Liu J, Huo S, Kumar A, Wei T, et al. Size-dependent localization and penetration of ultrasmall gold nanoparticles in cancer cells, multicellular spheroids, and tumors in vivo. ACS Nano 2012; 6: 4483–93.

[14] Kojima C, Kono K, Maruyama K, Takagishi T. Synthesis of polyamidoamine dendrimers having poly(ethylene glycol) grafts and their ability to encapsulate anticancer drugs. Bioconjug Chem 2000; 11: 910–7.

[15] Kono K, Kojima C, Hayashi N, Nishisaka E, Kiura K, Watarai S, et al. Preparation and cytotoxic activity of poly(ethylene glycol)-modified poly(amidoamine) dendrimers bearing adriamycin. Biomaterials 2008; 29: 1664–75.

[16] Wang F, Wang YC, Dou S, Xiong MH, Sun TM, Wang J. Doxorubicin-tethered responsive gold nanoparticles facilitate intracellular drug delivery for overcoming multidrug resistance in cancer cells. ACS Nano 2011; 5: 3679–92.

[17] G Frens. Controlled nucleation for the regulation of the particle size in monodisperse gold suspensions. Nat Phys Sci 1973; 241: 20–2.

[18] Chan W.C, White P.D. Eds. Fmoc solid phase peptide synthesis. Oxford University Press: New York; 2000, p. 41–76.

[19] Usui K, Tomizaki K, Mihara H. Protein-fingerprint data mining of a designed α-helical peptide array. Mol Biosyst 2006; 2: 417–20.

[20] Usui K, Kakiyama T, Tomizaki KY, Mie M, Kobatake E, Mihara H. Cell fingerprint patterns using designed α-helical peptides to screen for cell-specific toxicity. Bioorg Med Chem Lett 2011; 21: 6281–4.

[21] Usui K, Tomizaki K-Y, Mihara H. Screening of α-helical peptide ligands controlling a calcineurin-phosphatase activity. Bioorg Med Chem Lett 2007; 17: 167–71.

[22] Niidome T, Yamagata M, Okamoto Y, Akiyama Y, Takahashi H, Kawano T, et al. PEG-modified gold nanorods with a stealth character for in vivo applications. J Control Release 2006; 114: 343–7.

[23] Veronese FM, Pasut G. PEGylation, successful approach to drug delivery. Drug Discov Today 2005; 10: 1451–8.

[24] Zuco V, Supono R, Righetti SC., Cleris L, Marchesi E, Gambacorti-Passerini C, et al. Selective cytotoxicity of betulinic acid on tumor cell lines, but not on normal cells. Cancer Letters 2002; 175: 17–25.

Chapter 5.

Conclusions and future prospects

5-1 Conclusions and future prospects

Intracellular drug delivery systems are promising methods for human disease care, especially cancer therapy improving chemotherapy efficacy and reducing side effects of drugs. The construction of effective intracellular drug delivery systems has been studied using various vectors such as viral vectors [1] and non-viral vectors [2], such as liposome, cationic polymers and cell penetrating peptides (CPPs) [3-6]. Among them, the CPP-based intracellular delivery system has several advantages, such as easiness of synthesis or possibility of sequences modification. In this thesis, a cell-selective intracellular delivery system was constructed using α-helical CPPs developed in Mihara group and gold nanophere (GNS) and was evaluated their applicability.

In the chapter 2, the four kinds of α-helix peptides nanoprobes was constructed with two different peptides (EF and EA peptides) from an α-helix peptide library of Mihara group [7-10] conjugating at N-terminus or C-terminus to GNSs. Their peptide binding ability according to GNS size (10, 16, 25, 41 nm) was also evaluated. Among them, GNS41 conjugated the largest amount of peptide per particle and peptides-conjugated GNS41 (P-GNS41) showed the low cytotoxicity against HeLa cell, indicating high biocompatibility.

In the chapter 3, CP activity and cell death induction was evaluated using four P-GNSs41 constructed in the chapter 2. Peptides EF and EA have only one amino acid difference (Phe vs. Ala in the center of the sequence), however, they showed characteristic CP selectivity with three types of cells. In addition, selective cell death activity was induced using an anti-cancer drug, doxorubicin (DOX), conjugated to the P-GNSs41. P-DOX-GNSs41 showed enhanced cell-selective death induction compared with free DOX in solution and DOX-GNS41 without peptides, which was attributed to the cell-selective

penetrating activity of peptides EF and EA.

In the chapter 4, five nanoprobes by conjugating either the TAT peptide or one of four α-helical peptides, RF, RA, EF, and EA, to a 25 nm GNS were constructed. The four α-helical peptide-conjugated nanoprobes showed similar CP and cell death activities compared with the TAT peptide in three cell lines, with high cell selectivity according to cell type and peptide sequence. Moreover, P-DOX-PEG-GNS25, which contained a pH-sensitive DOX linkage, showed levels of cell death induction by DOX (20%-40%) that were approximately two times higher than those (10%-20%) constructed in the chapter 3, P-DOX-GNS41 [11].

These data indicate that constructed P-GNS systems have high cell selectivity, high efficiency, and low cytotoxicity. It could be applied to the development of 1) disease diagnosis 2) therapy 3) molecular imaging 4) cell-selective drug delivery, and 5) in vivo study. Drugs or target molecules of diseases immobilized P-GNS would be a useful element for molecular imaging, disease diagnosis, and therapy application. Because the P-GNS system was already succeeded in the cell-selective drug delivery of anti cancer drug, it would be expected to cancer therapy and in vivo application.

There are several tasks to examine for efficient applications of P-GNS nanoprobes. 1) Immunogenicity and toxicity: The constructed P-GNS system showed the high biocompatibility in vitro, however, high concentration may be needed for delivery in vivo system. The α-helical peptides showed the toxicity with high concentration [7-10], and a paper reported that GNS has lethal effect on mice [12]. The constructed P-GNS is needed to examine the cytotoxicity and immunogenicity in vivo conditions. 2) Clarification of cellular uptake mechanism: P-GNS was uptaken by endocytosis, however, detailed mechanisms of the internalization of α-helical peptides in Mihara group have not been well

understood. High selective and efficient system could be constructed according to clarification of the detail uptake mechanisms and uptake differences by amino acid sequences. 3) Stability in blood: P-GNS was stable in OPTI-MEM and PBS buffer for several months. For in vivo application, the P-GNS system should be examined in the stability of P-GNS and drug degradation in blood. 4) More efficient nuclear delivery than P-PEG-GNS25 system: P-PEG-GNS25 accumulated around the nucleus. Using this system, the effective cell selective drug delivery system was constructed. A higher nuclear delivery may be required for the improvement of efficiency of drug in vivo. These studies will improve the P-GNS system leading to the realization of in vivo applications.

Reference

[1] Thomas C.E., Ehrhardt A., Kay M.A. Progress and problems with the use of viral vectors for gene therapy. Nat rev Genet 2003; 4: 346-58.

[2] Niidome T, Huang L. Gene therapy progress and prospects: Nonviral vectors. Gene Ther 2002; 9: 1647-52.

[3] Lindgren M, Hällbrink M, Prochiantz A, Langel Ü. Cell-penetrating peptides. Trends Pharmacol Sci 2000; 21: 99-103.

[4] Hansen M, Kilk K, Langel Ü. Predicting cell-penetrating peptides. Adv Drug Deliver Rev 2008; 60: 572-9.

[5] Futaki S. Membrane-permeable arginine-rich peptides and the translocation mechanism. Adv Drug Deliver Rev 2005; 57: 547-58.

[6] Jiang T, Zhang Z, Zhang Y, Lv H, Zhou J, Li C, et al. Dual-functional liposomes based on pH-responsive cell-penetrating peptide and hyaluronic acid for tumor-targeted anticancer drug delivery. Biomaterials 2012; 33: 9246–58.

[7] Usui K, Kikuchi T, Mie M, Kobatake E, Mihara H. Systematic screening of the cellular penetration of designed alpha-helix peptides. Bioorg Med Chem 2013; 21: 2560–7.

[8] Usui K, Tomizaki K, Mihara H. Protein-fingerprint data mining of a designed α-helical peptide array. Mol Biosyst 2006; 2: 417–20.

[9] Usui K, Kakiyama T, Tomizaki KY, Mie M, Kobatake E, Mihara H. Cell fingerprint patterns using designed α-helical peptides to screen for cell-specific toxicity. Bioorg Med Chem Lett 2011; 21: 6281–4.

[10] Usui K, Tomizaki K-Y, Mihara H. Screening of α-helical peptide ligands controlling a calcineurin-phosphatase activity. Bioorg Med Chem Lett 2007; 17: 167–71.

[11] Park H, Tsutsumi H, Mihara H. Cell penetration and cell-selective drug delivery using

α-helix peptides conjugated with gold nanoparticles. Biomaterials 2013; 34: 4872–9.

[12] Chen Y, Hung Y, Lian I, Huand G.S. Assessment of the in vivo toxicity of gold nanoparticles. Nanoscale Res Lett 2009; 4: 858–864.

Acknowledgement

First I would like to express my sincere gratitude to my advisor Professor Hisakazu Mihara, who has supported me with his patience and knowledge.

I would also like to thank Assistant Professor Hiroshi Tsutsumi and Mihara Lab members for their encouragement, guidance and helpful suggestions.

Last but not least, thanks to all my family, my parents and brother for their patient love enabled me to complete this work.

저의 결정을 믿어주시고 지지해주신 사랑하는 부모님께 감사 드립니다. 그리고 묵묵히 동생을 지켜봐 주고, 힘이 되어준 오빠에게도 정말 고맙습니다.

또한 4년 반 동안 많은 격려와 힘이 되어준 분들과 친구들, 윤경이, 병희, 성숙씨, 찬엽 오빠, 성옥언니에게도 감사 드립니다.

같이 일본에서 공부하며 곁에서 큰 힘이 되어준 주연, 현보, 심 너무 고마워.

모든 분들의 격려와 도움으로 이 논문을 쓸 수 있었습니다. 다시 한번 감사 드립니다.

Papers

In this thesis

1) Park H, Tsutsumi H, Mihara H. Cell penetration and cell-selective drug delivery using α-helix peptides conjugated with gold nanoparticles. Biomaterials 2013; 34: 4872–9.

2) Park H, Tsutsumi H, Mihara H. Cell-selective intracellular drug delivery using doxorubicin and α-helical peptides conjugated to gold nanoparticles. Biomaterials 2014; 35: 3480–8.

Others

1) Park H, Lee M, Seong GH, Choo J, Lee EK, Park JY, et al. Open sandwich FRET immunoassay of estrogen receptor β in a PDMS microfluidic channel. Bull Korean Chem Soc 2008; 29: 1297–8.

2) Park H, Lee S, Chen L, Lee EK, Shin SY, Lee YH, et al. SERS imaging of HER2-overexpressed MCF7 cells using antibody-conjugated gold nanorods. Phys Chem Chem Phys 2009; 11: 7444–9.

3) Tsutsumi H, Ohkusa H, Park H, Takahashi T, Yuasa H, Mihara H. Gold nanoparticles conjugated with monosaccharide-modified peptide for lectin detection. Bioorg Med Chem Lett 2012; 22: 6825–7.

Presentations at conference

In this thesis

1) Hyejin Park, Takuya Kikuchi, Tsuyoshi Takahashi, Hisakazu Mihara

Cell Penetrability with α-Helical Peptides Conjugated with Gold Nanospheres and Detection Using Dark Field Microscopy"

5th International Peptide Symposium, Kyoto International Conference Center (2010.12.4-9)

2) Hyejin Park, Tsuyoshi Takahashi, Hisakazu Mihara

金ナノ粒子に結合したαヘリックスペプチドの細胞導入活性

日本化学会第91春季年会，神奈川大学 (2011.3.26-29)

3) Hyejin Park, Tsuyoshi Takahashi, and Hisakazu Mihara

金ナノ粒子に結合した αヘリックスペプチドの細胞導入活性

第5回日本化学会関東支部，東京農工大学 (2011.8.30-31)

4) Hyejin Park, Tsuyoshi Takahashi, and Hisakazu Mihara

Cell Penetrability and Application of α-Helical Peptides Conjugated with Gold Nanoparticles

第5回バイオ関連化学シンポジウム，つくば国際会議場 (2011.9.12-14)

5) Hyejin Park, Tsuyoshi Takahashi, Hiroshi Tsutsumi, Hisakazu Mihara

Cell Penetration and Application of α-Helical Peptides Conjugated with Gold Nanoparticles

第48回ペプチド討論会，札幌コンベンションセンター (2011.9.26-29)

6) Hyejin Park, Hiroshi Tsutsumi, Hisakazu Mihara

Cell Penetration and Application of α-Helical Peptides Conjugated with Gold Nanoparticles

The 15th Korean Peptide Protein Symposium, Ochang, South Korea (2011.12.1)

Award: 1) 2011 Young Scientist Award, 2) JPS Travel Award

7) Hyejin Park, Tsuyoshi Takahashi, Hiroshi Tsutsumi, Hisakazu Mihara

α ヘリックス細胞挿入ペプチド-金ナノ粒子複合体は、低濃度で細胞導入される

第14回生命化学研究会，ラフォーレ南紀白浜 (2011.12.2-3)

8) Hyejin Park, Hiroshi Tsutsumi, Hisakazu Mihara

Drug Delivery using α-helical Peptide Conjugated Gold Nanoparticles with Cell Penetrating Activity

The Second Asian Chemical Biology Conference, Okinawa, Japan (2012.7.4-6)

9) Hyejin Park, Hiroshi Tsutsumi, Hisakazu Mihara

Cell Penetration and Cell Selective Drug Delivery using α-helical Peptides Conjugated with Gold Nanoparticles

第49回ペプチド討論会，かごしま県民交流センター (2012.11.7-9)

10) Hyejin Park, Hiroshi Tsutsumi, Hisakazu Mihara

Cell Selective Drug Delivery using Cell Penetrating alpha-Helix Peptides Conjugated with Gold Nanoparticles

The First International Symposium on Biofunctional Chemistry, Tokyo Tech (2012.11.28-15)

11) Hyejin Park, Hiroshi Tsutsumi, Hisakazu Mihara

細胞透過ペプチドと金ナノ粒子を用いた細胞選択的ドラックデリバリ

第7回バイオ関連シンポジウム，名古屋大学 (2013.9.27-29)

Others

1) Hyejin Park, Byoung Hee Han, Moonkwon Lee, Jaebum Choo

Molecular Imaging of MCF7 Cells Expressing HER-2 Cancer Markers Using Dark-field and Fluorescence Emission Microscopy

The 100th National Meeting of Korean Chemical Society, Seoul, South Korea (2007.10.18-19)

2) Moonkweon Lee, Linaxin Chen, Ly Xuan Quang, Hyejin Park, Jaebum Choo

Fast DNA Hybridization Analysis Using Optical Microfluidic Sensor

The 9th Asian Conference on Analytical Sciencesl, Jeju, South Korea (2007.11.4-7)

3) Hyejin Park, Moonkwon Lee, Chaesung Lim, Jaebum Choo

Development of an Open Sandwich FRET Immunoassay in a Microfluidic Channel

The 101st National Meeting of Korean Chemical Society, Ilsan City, South Korea (2008. 4.17-18)

4) Hyejin Park, Jaebum Choo

Molecular Imaging of MCF7 Cells Expressing HER-2 Cancer Markers Using Gold Nanorod-based SERS Imaging

The 2008 Korea-Japan Symposium on Frontier Photoscience, Jeju, South Korea (2008.9.25-28) Poster Presentation Award

5) Hyejin Park, Jaebum Choo

Molecular Imaging of MCF7 Cells Expressing HER-2 Cancer Markers Using Gold Nanorod Based SERS Imaging

The 8th International Drug Discovery Science and Technology, Beijing, China (2008.10.18-22)

6) Hiroyuki Okusa, Hyejin Park, Hideya Yuasa, Hisakazu Mihara

単糖導入ペプチド修飾金ナノ粒子とレクチンとの相互作用

第5回日本化学会関東支部，東京農工大学 (2011.8.30-31)

7) Hiroyuki Okusa, Hyejin Park, Hideya Yuasa, Hisakazu Mihara

レクチンに対する結合多様性を有する単糖導入ペプチド修飾金ナノ粒子の創製

第5回バイオ関連化学シンポジウム，つくば国際会議場 (2011.9.12-14)

8) Hiroyuki Okusa, Hyejin Park, Hideya Yuasa, Hisakazu Mihara

単糖導入ペプチド修飾金ナノ粒子を利用したレクチンの検出

第48回ペプチド討論会，札幌コンベンションセンター (2011.9.26-29)

9) Hiroyuki Okusa, Hyejin Park, Hideya Yuasa, Hisakazu Mihara

単糖導入ペプチド修飾金ナノ粒子の構築とレクチンへの結合多様性の獲得

日本化学会第92春季年会，慶應義塾大学 (2012.3.25)